VOL. 1 No. 6
DECEMBER 1959

URNAL OF THE

LESS-COMMON METALS

UNIVERSITY OF HAWAII
LIBRARY
FEB 8 1961

AN INTERNATIONAL JOURNAL ON
THEIR CHEMISTRY AND METALLURGY

TORS:
. CUTHBERTSON (Nottingham)
AIRBROTHER (Manchester)

TORIAL ADVISORY BOARD:
NARD (Paris)
JRICE COOK (Birmingham)
ECROLY (Brussels)
DJINGHEUZIAN (Ottawa)
. FLETCHER (Harwell)
. GONSER (Columbus, Ohio)
IANSEN (Frankfurt a.M.)
NDELLI (Genoa)
LEMM (Münster)
. KROLL (Corvallis, Ore.)
URRAY (Harwell)
OWOTNY (Vienna)
. PIDGEON (Toronto)
. POWELL (Wembley)
. RALSTON (Hyattsville, Md.)
. VAN ARKEL (Leyden)
. WORNER (Melbourne)
YNTEMA (Menlo Park, Calif.)

ELSEVIER

GENERAL INFORMATION

Types of contributions

(a) Original research work not previously published in other periodicals.
(b) Reviews on recent developments in various fields.
(c) Short communications.
(d) Bibliographical notes and book reviews.

Languages

Papers will be published in English, French or German.

Submission of papers

Papers should be sent to one of the following Editors:

Professor J. W. CUTHBERTSON (*Metallurgy*), Department of Metallurgy, The University, University Park, Nottingham, England.
Professor F. FAIRBROTHER (*Chemistry*), The University of Manchester, Department of Chemistry, Manchester 13, England.

Authors should preferably submit two copies in double-spaced typing on pages of uniform size. Legends for figures should be typed on a separate page. The figures should be in a form suitable for reproduction, drawn in Indian ink on drawing paper or tracing paper, with lettering etc. in thin pencil. The sheets of drawing or tracing paper should preferably be of the same dimensions as those on which the article is typed. Photographs should be submitted as clear black and white prints on glossy paper.
All references should be given at the end of the paper. They should be numbered and the numbers should appear in the text at the appropriate places.
A summary of 50 to 200 words should be included. Authors of papers in French or German are encouraged to supply also a translation of the summary in English.

Reprints

Twenty-five reprints will be supplied free of charge. Additional reprints can be ordered at quoted prices. They must be ordered on order forms which are sent together with the proofs.

Publication

The *Journal of the Less-Common Metals* will have six issues to the volume, approx. 500 pages per volume.
Subscription price: £ 5.7.6 or $ 15.— or Dfl. 57.— per volume (post free).
For advertising rates apply to the publishers.

Subscriptions

Subscriptions should be sent to:

ELSEVIER PUBLISHING COMPANY, Spuistraat 110-112, Amsterdam-C., The Netherlands.

UNTERSUCHUNGEN AN NIOB-TANTAL-LEGIERUNGEN

H. BRAUN, K. SEDLATSCHEK UND R. KIEFFER

Metallwerk Plansee A.G., Reutte/Tirol (Österreich)

(Eingegangen den 29. Oktober 1959)

ZUSAMMENFASSUNG

Niob–Tantal-Sinterlegierungen über den ganzen Bereich des Systems wurden im verformten Zustand auf Härte, Zugfestigkeit, Streckgrenze, Dehnung, spezifische elektrische Leitfähigkeit sowie auf ihr elektrochemisches Verhalten und ihre Korrosionsbeständigkeit untersucht. Sie zeigen hinsichtlich ihrer mechanischen Eigenschaften ein vermittelndes Verhalten. Die spez. elektrische Leitfähigkeit besitzt ein Minimum bei mittlerer Konzentration, der Reststrom anodisch oxydierter Legierungsproben verläuft mit Maximum.

Derartige Legierungen, die aus verhältnismässig billigem, ungetrennten Niob–Tantal-Pulver hergestellt werden könnten, kommen als Heizleiterwerkstoff in Frage. Bei Verwendung in Elektrolytkondensatoren oder in der chemischen Industrie darf der Niobgehalt gewisse Grenzen nicht übersteigen.

SUMMARY

Sintered and subsequently rolled niobium – tantalum alloys are examined over the whole range of composition. Their hardness, strength and elongation at room temperature, their specific electrical conductivity, electrochemical behaviour and corrosion resistance are reported. The mechanical properties show no maximum. The specific electrical conductivity has a minimum and the leakage current of anodically anodised samples exhibits a maximum at an alloy concentration of 50Nb/50Ta.

Such alloys which might be fabricated from inexpensive unseparated niobium – tantalum powder represent advantageous heating element material for vacuum furnaces. Their application as electrodes for electrolytic capacitors and in the chemical industry requires low niobium contents of the alloys.

EINLEITUNG

Die Anwendung hochschmelzender Metalle und Legierungen hat in den letzten Jahren an Umfang immer mehr zugenommen. Insbesondere haben die Metalle Tantal und Niob eine starke Ausweitung ihrer bisherigen Verwendungsgebiete gefunden, was auf ihren hohen Schmelzpunkt, ihre günstigen elektrischen Eigenschaften und vor allem auf ihre ausgezeichnete Korrosionsbeständigkeit zurückzuführen ist, wobei das Tantal dem Niob überlegen ist.

Die enge Vergesellschaftung von Niob und Tantal in ihren Erzen und ihr ähnliches chemisches Verhalten erfordern eine komplizierte nasschemische Trennung der beiden Elemente. Der dadurch bedingte hohe Preis der Metalle liess es wünschenswert erscheinen, Niob–Tantal-Legierungen auf ihre physikalischen und mechanischen Eigenschaften zu untersuchen und auf Grund der Ergebnisse zu prüfen, ob derartige Legierungen für Anwendungen in Frage kommen, die bisher den reinen Metallen

Literatur S. 419

vorbehalten waren. Die Verwendung von unvollständig bzw. ungetrenntem Tantal–Niobpulver würde derartige Legierungen nämlich bedeutend verbilligen.

Die in der Literatur vorhandenen Angaben von H. BÜCKLE[1] und D. E. WILLIAMS und W. H. PECHIN[2] zeigen die lückenlose Mischkristallbildung im System Niob–Tantal, geben aber keine Anhaltspunkte über die mechanischen und chemischen Eigenschaften der Legierungen.

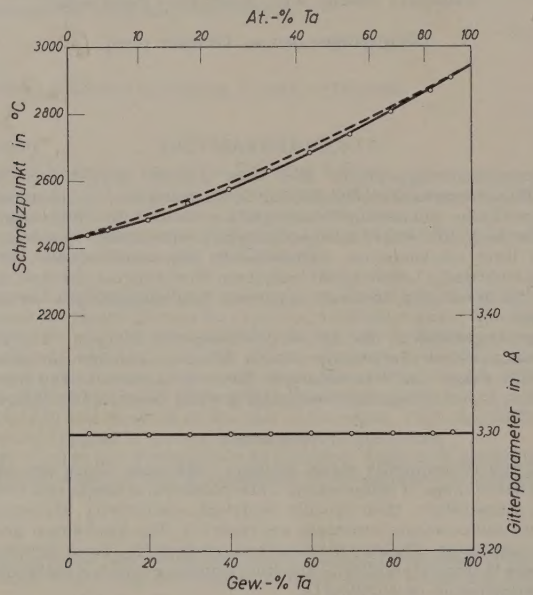

Abb. 1. Das Zustandsdiagramm Niob – Tantal (D. E. WILLIAMS UND W. H. PECHIN).

Abb. 1 zeigt das Zustandsschaubild von Niob – Tantal[2], wie es auf Grund röntgenographischer und metallographischer Untersuchungen sowie von Widerstandsmessungen aufgestellt wurde.

HERSTELLUNG DER LEGIERUNGEN

Ausgangspulver

Die auf eine Korngrösse von $< 60\ \mu$ ausgesiebten, aus Tantal-, bzw. Niobhydrid durch Vakuumentgasung erhaltenen Pulver hatten die in Tabelle I aufgeführten Hauptverunreinigungen.

Sintern und Verformen

Pulveransätze mit 20, 40, 60 und 80 At.-%* Tantal sowie auch die Reinmetalle wurden zu Proben von $10 \times 10 \times 75$ mm verpresst und in einem Hochvakuumofen mit Tantalheizleiter bei etwa 3×10^{-5} torr 10 Stunden bei 2000°C gesintert.

* Alle Angaben in Atom-%

Literatur S. 419

TABELLE I

CHEMISCHE ANALYSE DER AUSGANGSPULVER

Hauptbestandteile und Verunreinigung	*Tantal* %	*Niob* %
Stickstoff	n.b.	0.056
Kohlenstoff	0.01	0.04
Eisen	0.013	0.037
Wolfram	0.06	—
Molybdän	0.11	—
Niob	0.32	98.3
Tantal	99.4	1.48
DR*	0.02	0.02

* Destillationsrückstand im Chlorstrom.

Der Sinterlängsschwund betrug einheitlich etwa 16%. Die Sinterkörper wurden mit einer Zwischenglühung bei 2.6 mm Stärke (30 min/1160°C) auf 0.25 mm-Blech quer weiter gewalzt, bei 1170°C, 35 min endgeglüht und an diesem die Untersuchungen durchgeführt.

Untersuchungsmethoden

Die *Härte* wurde an den gesinterten und gewalzten Legierungen (walzhart und nach Schlussglühung (35 min/1170°C)) gemessen. *Zugfestigkeit, Streckgrenze* und *Dehnung* wurde an geglühten Blechproben mit einer Belastungsgeschwindigkeit von 1 kg/sec bestimmt.

Die *spezifische elektrische Leitfähigkeit* wurde nach dem Wirbelstromverfahren an 2.6 mm dicken Blechproben ermittelt (Sigmatest der Fa. Foerster, Reutlingen).

Das *Formierverhalten* (anodische Oxydation) wurde an vorher gebeizten Blechproben 20 × 40 mm untersucht. Die Bedingungen waren folgende:

Elektrolyt	0.1% Phosphorsäure
Temperatur	90°C
Spannung	200 V
Formierdauer	30 minuten.

Die Messung von *Kapazität* und *Reststrom* anodisch oxydierter Proben erfolgte im selben Elektrolyten bei Raumtemperatur nach einer 2-minutigen Nachformierung bei 180°C. Die Kapazitätsmessung wurde bei einer Messfrequenz von 120 Hz durchgeführt.

Das *Korrosionsverhalten* wurde in statischen Versuchen ermittelt. Die Einwirkungsdauer der angreifenden Medien betrug durchwegs 96 Stunden.

Versuchsergebnisse

Entsprechend der für tantalreiche Legierungen niedrigen Sintertemperatur von 2000°C wurden mit steigendem Tantalgehalt im Fertigblech steigende Sauerstoffgehalte an Hand des Oxydationswertes* festgestellt. Dieser Verlauf des Sauerstoffgehaltes in den Legierungen ist verantwortlich für den unerwartet starken Anstieg der

* Der Oxydationswert gibt das Gewicht einer 100 g-Metallprobe nach vollständiger Oxydation zum höchstwertigen Oxyd an.

Literatur S. 419

mechanischen Eigenschaften zu höheren Tantalgehalten hin, wie er für die Härte aus Tabelle II und Abb. 2, für die Zugfestigkeit und Streckgrenze aus Abb. 3 hervorgeht.

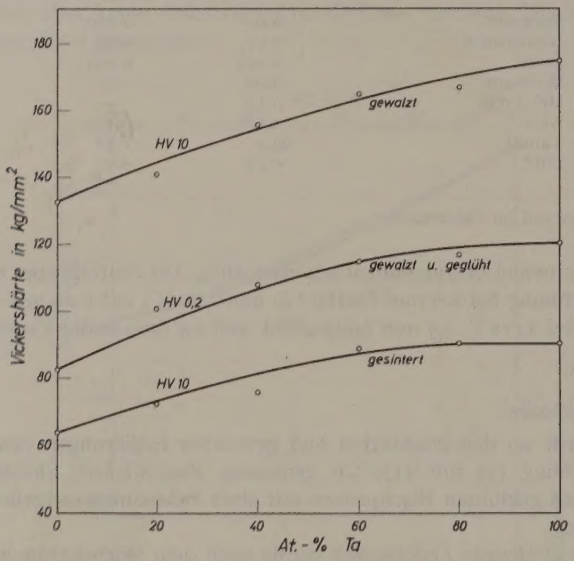

Abb. 2. Härte von Niob–Tantal-Legierungen.

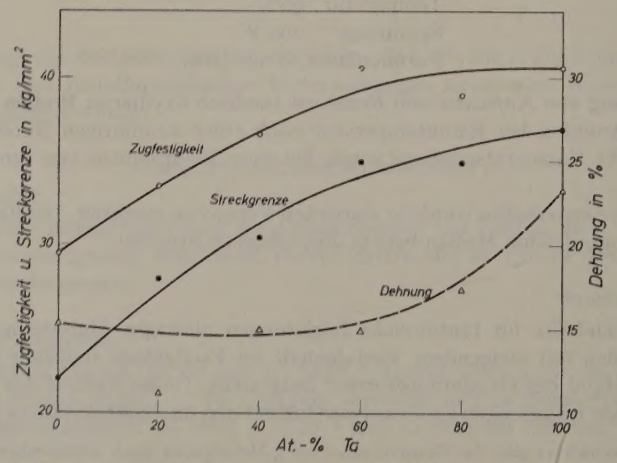

Abb. 3. Mechanische Eigenschaften von Niob–Tantal-Legierungen.

Literatur S. 419

TABELLE II

HÄRTE VON NIOB – TANTAL-LEGIERUNGEN VERSCHIEDENEN VERFORMUNGSGRADES

Ta At.-%	*gesintert 2000°/10 Std. HV 10 kg/mm²*	*längsgewalzt auf 2.6 mm, walzhart geglüht 1160°C/30 min HV 10 kg/mm²*		*quergewalzt auf 0.25 mm, geglüht 1170°C/ 35 min HV 0.2 kg/mm²*
0(Nb)	64.0	133	91	83
20	72.5	141	128	104
40	76.0	156	131	106
60	89.0	165	155	115
80	90.5	167	114	117
100 (Ta)	90.5	175	111	121

Härte, Zugfestigkeit, Streckgrenze und Dehnung verlaufen zwischen den reinen Komponenten vermittelnd. Ein Ansteigen des Streckgrenzenverhältnisses mit steigendem Tantalgehalt steht in Zusammenhang mit dem oben erwähnten zunehmenden Sauerstoffgehalt. Dass trotzdem die Dehnungswerte ebenfalls ansteigen, ist vielleicht so zu erklären, dass die an sich höhere Übergangstemperatur des Niobs (etwa —120°C) durch Mischkristallbildung stark erhöht wird und damit der Steilabfall der Duktilitäts-Temperaturkurve niobreicher Legierungen schon in den Bereich der Prüftemperatur (20°C) fällt. Tantal, dessen Übergangstemperatur bedeutend unterhalb —200°C liegt, wird hingegen durch Mischkristallbildung wenig verschlechtert, die gute Dehnung bleibt erhalten (vergl. Abb. 3).

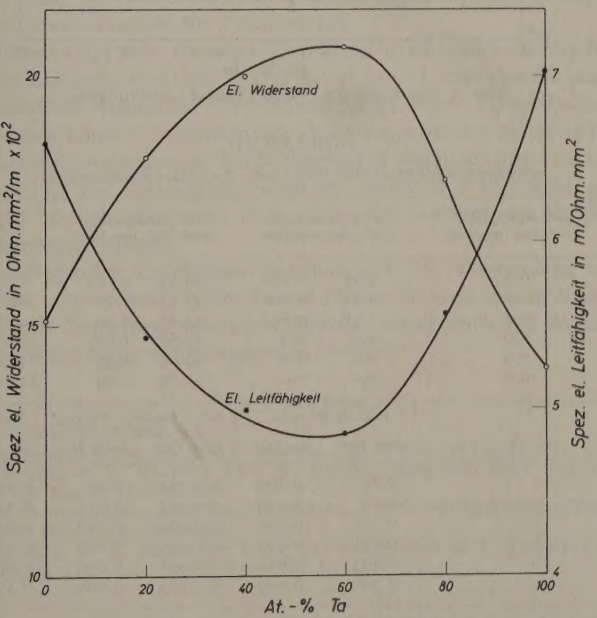

Abb. 4. Spezifische elektrische Leitfähigkeit und Widerstand von Niob–Tantal-Legierungen.

Literatur S. 419

Die *spezifische elektrische Leitfähigkeit* zeigt ein Minimum zwischen 40 und 60 At.-% Tantal (Abb. 4), sie fällt für eine Legierung 50/50 gegenüber Niob um etwa 40%, gegenüber Tantal um etwa 47% ab.

Das *Formierverhalten* der untersuchten Legierungen, wurde durch die Kapazität und den Reststrom nach anodischer Oxydation unter den früher beschriebenen Bedingungen ausgedrückt (Abb. 5). Bei einer für alle Proben gleichbleibenden Kapazität

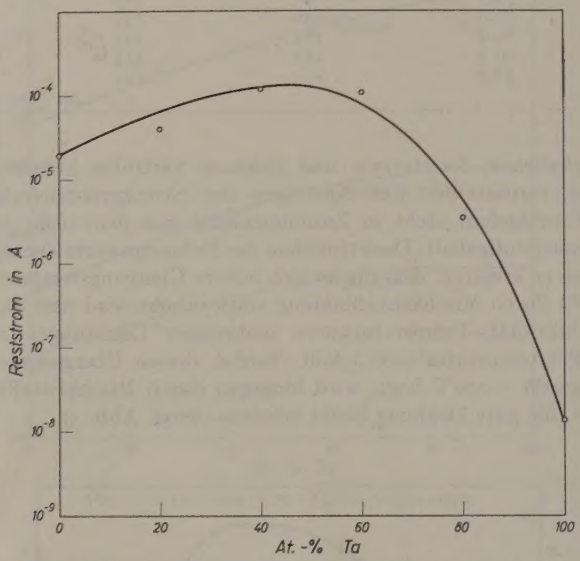

Abb. 5. Reststrom von Niob–Tantal-Legierungen.

TABELLE III

KORROSIONSVERHALTEN VON NIOB–TANTAL-LEGIERUNGEN

At.-% Ta	20% H_2SO_4, 20°C g/m², Tag	mm/Jahr	20% KOH, 20°C g/m², Tag	mm/Jahr	20% HF, 20°C g/m², Tag	mm/Jahr	20% HF + 200g NH_4F/l, 20°C g/m², Tag	mm/Jahr
0 (Nb)	0.0		4.35	0.180	16.93	0.704	13.52	0.562
20	0.0		3.12	0.100	37.53	1.20	26.30	0.840
40	0.0		1.16	0.032	51.22	1.40	41.60	1.14
60	0.0		0.0	0.0	55.87	1.37	61.50	1.52
80	0.0		0.0	0.0	59.00	1.35	76.40	1.75
100 (Ta)	0.0		0.0	0.0	105.80	2.29	123.20	2.67

	10% NaOH, 50°C g/m², Tag	mm/Jahr	$H_2SO_4 - Na_2SO_4 - ZnSO_4$,* 50°C g/m², Tag	mm/Jahr	Chromschwefelsäure, 100°C g/m², Tag	mm/Jahr
0 (Nb)	2.87	0.160	+0.364	0.02	0.614	0.034
20	1.23	0.039	+0.344	0.011	0.541	0.017
40	0.737	0.020	+0.364	0.010	0.654	0.018
60	0.939	0.023	+0.379	0.009	0.513	0.013
80	0.493	0.011	+0.438	0.010	0.689	0.016
100 (Ta)	0.396	0.009	+0.283	0.006	0.477	0.010

* 105 g H_2SO_4 konz. + 320 g Na_2SO_4 + 10 g $ZnSO_4$/l, ähnlich einem Viskosespinnbad.

Literatur S. 419

von 0.7—0.8 μF erweisen sich nur die tantalreichen Legierungen bis etwa 10–15 At.-% Niob as Elektrodenmaterial für Elektrolytkondensatoren verwendbar, da nur diese Reststromwerte den Anforderungen entsprechen.

Tabelle III gibt das Ergebnis der *Korrosionsversuche* wieder. Gegen 20%ige Schwefelsäure sind alle Zusammensetzungen beständig. Der Angriff durch 20%ige Kalilauge unter Luftzutritt beschränkt sich auf die niobreichen Legierungen bis 60 At.-% Niob. Die Korrosion in Flusssäure und im Flusssäure–Ammonfluoridgemisch bestätigt die Angaben von B. FETKENHEUER[3] und F. RITTER[4], nach denen Niob gegenüber Flusssäure und Fluoride enthaltende Lösungen beständiger ist als Tantal. Die Untersuchungen bei höheren Temperaturen wurden mit jenen angreifenden Medien durchgeführt, welche für die Überprüfung von Spinndüsenmaterial verwendet werden[5]. Sowohl in der Viskose (ersetzt durch 10% Natronlauge bei 50°C) als im Spinnbad ($H_2SO_4 - Na_2SO_4 - ZnSO_4$ bei 50°C) und Reinigungsbad (Chromschwefelsäure bei 100°C) ist das Tantal dem Niob und niobreichen Legierungen überlegen.

DISKUSSION DER ERGEBNISSE

Eine erste technologische Untersuchung im System der voll mischbaren Metalle Niob–Tantal zeigt, dass bei ausgezeichneter Verformbarkeit aller Zusammensetzungen keine Maxima von Härte und Festigkeit auftreten, vielmehr verlaufen diese Eigenschaften vermittelnd zwischen den reinen Komponenten, ähnlich wie im System Molybdän–Wolfram[6].

Die spezifische elektrische Leitfähigkeit zeigt ein ausgeprägtes Minimum; nachdem damit immer auch ein Minimum im Verlauf des Temperaturkoeffizenten des Widerstandes verbunden ist, sind Niob–Tantal-Legierungen mittlerer Zusammensetzung günstige Heizleiterwerkstoffe für Vakuumöfen.

Im allgemeinen zeigt sich, dass das Niob hinsichtlich seiner chemischen und elektrochemischen Eigenschaften dem Tantal unterlegen ist, dass aber für einige Fälle, wo heute ausschliesslich Reintantal Verwendung findet, Niob–Tantal-Legierungen auch eingesetzt werden können, beispielsweise als korrosionsfestes Material im Apparatebau, für Elektrolytkondensatoren bei Niobgehalten von nicht mehr als 10 – 15 At.-% (5.5 – 8.5 Gew.-%) für Spinndüsen, wenn ein Niobgehalt von etwa 40 At.-% (25 Gew.-%) nicht überschritten wird, und, wie bereits erwähnt, als Heizleitermaterial in allen Zusammensetzungen.

Mit den vorliegenden Ergebnissen zeichnet sich die Verwendung unvollständig getrennter bzw. ungetrennter Niob–Tantal-Pulver ab, was sich in einer erheblichen Preissenkung der Legierung auswirken könnte, wobei auch die Aufarbeitung des Legierungsschrottes keine Schwierigkeiten bereitet.

LITERATUR

1 H. BÜCKLE, *Z. Metallk.*, 37 (1946) 53.
2 D. E. WILLIAMS UND W. H. PECHIN, *Trans. Am. Soc. Metals*, 50 (1958) 1081.
3 B. FETKENHEUER, in R. KIEFFER UND W. HOTOP, *Pulvermetallurgie und Sinterwerkstoffe*, Springer-Verlag, Berlin, 1943, S. 266.
4 F. RITTER, *Korrosionstabellen metallischer Werkstoffe*, 4. Aufl., Springer-Verlag, Wien, 1958, S. 101.
5 H. HOLZMANN, *Persönliche Mitteilung*.
6 M. H. LA CHANCE, W. L. BRUCKART, C. M. CRAIGHEAD UND R. I. JAFFEE, *Trans. Am. Soc. Metals*, 45 (1953) 314.

THE RECOVERY OF RHENIUM AND THE ANALYSIS OF ITS ALLOYS

A. A. WOOLF

Research Laboratory, Associated Electrical Industries, Aldermaston, Berks. (Great Britain)

(Received December 29th, 1959)

SUMMARY

The quantitative recovery of rhenium from analytical or other residues by conversion to ammonium perrhenate on ion exchange columns, followed by hydrogen reduction or thermal decomposition of ammonium hexaiodorhenate is described. A simple static oxidation method has been used to analyse a number of binary and ternary alloys.

In view of the current interest in rhenium and its alloys[1] an account of our experience in analysing and recovering rhenium from alloys, may be helpful for others who work with gram quantities of the metal.

PREPARATION OF THE METAL

Potassium perrhenate is the usual source of metallic rhenium, and analytical residues contain either this salt or the sodium one. A typical procedure for recovery of metal from the potassium salt[2] is to reduce by hydrogen at 550°C and leach the residue with water to remove alkali. A further reduction at 1000°C is followed by leaching with dilute hydrochloric acid and water and a final reduction at 1000°C. The metal so produced is reconverted to the heptoxide with oxygen at 800°C, the volatilised oxide dissolved in water, and then precipitated as ammonium perrhenate with gaseous ammonia. This somewhat lengthy procedure is necessary because the metal produced from potassium perrhenate is always contaminated with potassium even after the double leaching. We find that the reduction of the potassium salt is far from quantitative and recovery of the unused salt is essential.

It is possible to simplify the above method by quantitative conversion of potassium to ammonium perrhenate on a cation exchange resin column. The reduction of the ammonium salt is facile and almost quantitative with no alkali contamination.

The only disadvantage of the exchange method is the need to evaporate large volumes of eluates because of the low solubility of potassium perrhenate. We tried two methods to avoid these evaporations. The first used cathodic reduction of acid solutions of potassium perrhenate, the second used zinc reduction. It was hoped that as the reaction progressed more salt would dissolve, and that the metal and metal oxide formed could then be dissolved in a minimum of hydrogen peroxide. However,

References p. 423

the current efficiency of the first process was too low, and the precipitate from the second too bulky and difficult to wash, for these methods to compete with the exchange method.

Another method for preparing the metal which avoids hydrogen reduction is by the decomposition of ammonium hexaiodorhenate $(NH_4)_2ReI_6$ in vacuo at 700°C, a process which proceeds via intermediate rhenium iodides[3]. The iodorhenate can be prepared quantitatively from ammonium perrhenate. Metal powder produced by this method shows no difference in mechanical properties, after consolidation by arc melting, over powder from the hydrogen reduction method, and the latter is therefore the preferred method.

An important practical point is the choice of material to contain the salt during reduction. Refractory metals such as tantalum or molybdenum have been recommended, but we find that either diffusional alloying or the reducing atmosphere present (including steam and cracked ammonia) embrittles these metals and it is difficult to exclude metal flakes when removing rhenium from these containers. Copper containers are much superior provided that adequate thickness of metal is taken to compensate for the softening of the metal. Reduced rhenium is cleanly separated from copper and it has been shown previously that no reaction occurs[4]. Silica is not recommended because it embrittles after continuous use and may contaminate the rhenium.

ANALYSIS OF RHENIUM ALLOYS

The choice of method is limited by the necessity to recover rhenium, and the desire to make it as universal as possible. A simple oxidation in a static atmosphere fulfils these requirements. Rhenium in most alloys is readily volatilized as the heptoxide which can be dissolved in water and titrated with standard alkali. Oxides which differ in volatility from rhenium oxide can often be separated simultaneously, and estimated by direct weighing or by subsequent solution methods. For example, after oxidation of a tantalum–molybdenum–rhenium alloy at 1000°C, the residual tantalum oxide can be weighed, the sublimed molybdenum oxide dissolved and precipitated with benzoin oxime, and rhenium oxide titrated alkalimetrically. The rates of oxidation of rhenium alloys in general decrease with decreasing volatility of the component oxides but non-adherent surface coatings prevent a simple linear or parabolic law from applying. In extreme cases such as rhenium–silicon alloys rich in silicon, the oxidation rate is too slow for the oxidation method to be practical.

The advantages of the method are that separations are more easily effected than with solution methods, the components are recovered as solids which can be dissolved in small volumes, the specimen can be in massive form, an important consideration with alloys whose mechanical properties prevent easy comminution, and finally the method could be adapted for micro quantities.

The following alloys have been analysed by the oxidation method: rhenium–carbon; rhenium–silicon; rhenium–niobium, rhenium–niobium–tungsten; rhenium–tantalum, rhenium–tantalum–molybdenum, rhenium–molybdenum-tungsten–tantalum; rhenium–molybdenum, rhenium–molybdenum–chromium, rhenium–molybdenum-tungsten–vanadium; rhenium–tungsten, rhenium–molybdenum–tungsten; (molybdenum–platinum, molybdenum–tungsten).

References p. 423

EXPERIMENTAL

Behaviour of potassium perrhenate on cation exchange columns

$KReO_4$ (0.6630 g of twice recrystallised salt) was passed through a column of Amberlite IR.120H (5 g) in the hydrogen form. The acid eluted required 22.90 ml of 0.1 *N* alkali for neutralization (calc. 22.91). The acid solution (0.03094 *M*) had a pH value 1.60 (calc. 1.59 from the ionic strength).

$KReO_4$ solution (0.2994 g/100 ml) was passed through a column in the ammonium form. The ammonium ion in the eluate was determined by heating with excess alkali and back titration with acid. Found 10.28 ml 0.1 *N* acid (calc. 10.33 ml).

These small scale experiments showed that perrhenate acid is a strong acid and that its salts can be quantitatively interconverted.

Large scale preparation of ammonium perrhenate

A glass column (4 cm diam. 150 cm long) with 450 g of 80 mesh Zeocarb 225 was conditioned with alternate solutions of 10% HCl and 10% NH_4Cl and finally left in the ammonium form. $KReO_4$ (60 g in 5 l) was passed through, followed by 3 l of water. Conductivity measurements showed less than 1 p.p.m. of rhenium in solution with the last washings. The NH_4ReO_4 solution was evaporated almost to dryness on a hot plate, and then to dryness in a steam bath under an infra-red lamp. Any slight decomposition which occurs, tinting the white salt blue, does not affect the purity of metal obtained on reduction (found 6.42 % NH_3, calc. 6.46). The bulk of solution could be reduced 5–6 fold by working the column at 60°C, but the complication of apparatus is hardly worthwhile on this scale.

Reduction of ammonium perrhenate

Oxygen-free hydrogen was passed over the salt in a copper boat in a silica tube and temperature gradually raised to 400°C and held for 3 h. The gas flow was observed in a water bubbler on the exit side, which also served to indicate when all the ammonia had been displaced. The temperature was then raised to 1000°C during 1 h and maintained for a further 2 h before the tube was allowed to cool in a hydrogen stream. Some examples of recoveries are:

$KReO_4$	NH_4ReO_4 recovered	% theory	Re recovered	% theory	Purity found	
60.3	54.9	100.0	37.0	95.4	100.2	± 0.2
60.0	54.9	100.5	38.1	98.6	100.2	
37.9	34.3	99.6	23.5	96.4	99.8	

The slight loss of rhenium is due to volatilisation and reduction of ammonium perrhenate outside the boat. Potassium perrhenate residues contaminated with chloride and sulphate can be treated in the same way. The ammonium chloride and sulphate formed, sublime away from the boat.

Analysis of alloys by oxidation

The apparatus (Fig. 1) consists of a horizontal silica tube containing the sample (alone or in a platinum foil capsule) joined to a 500 ml bulb. The bulb is evacuated and filled with oxygen to 1⅓ atmospheres, and the silica tube held at 1000°C until oxidation was completed. (Observed by the sublimate and residue.) The silica tube

References p. 423

was removed and cut just below the sublimed layer of rhenium oxide, the oxide residue in the platinum container could be removed and weighed. The rhenium oxide was dissolved in water and titrated with standard alkali to the methyl red end-point, alternatively spectrophotometric analysis at 2100 Å is possible[5].

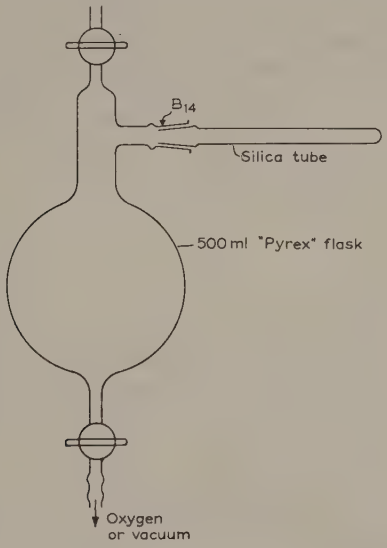

Fig. 1. Oxidation flask for alloy analysis.

The apparatus for rhenium -carbon analysis was different in that the silica tube was joined in line between the taps. The carbon dioxide formed was displaced by a stream of nitrogen, after allowing the apparatus to reach room temperature, into standard baryta solution.

ACKNOWLEDGEMENTS

The author wishes to thank Dr. G. A. GEACH for his encouragement and advice, and Dr. T. E. ALLIBONE, F.R.S., Director of the Laboratory, for permission to publish this paper.

REFERENCES

1 G. A. GEACH AND J. E. HUGHES, *Plansee Proc., Reutte/Tyrol*, 1955, (Pub. 1956) 245;
A. G. KNAPTON, *J. Inst. Metals*, 87 (1958–59) 28, 62;
A. G. KNAPTON, *Plansee Proc., Reutte/Tyrol*, 1958, (Pub. 1959) 412;
I. E. CAMPBELL, D. M. ROSENBAUM AND B. W. GONSER, *J. Less-Common Metals*, 1 (1959) 185.
2 Battelle Memorial Institute: *Report on Rhenium*, March, 1953.
3 R. D. PEACOCK, A. J. E. WELCH AND L. F. WILSON, *J. Chem. Soc.*, (1958) 2901;
A. A. WOOLF, *J. Inorg. & Nuclear Chem.*, 7 (1958) 291.
4 U. HOLLAND-NELL AND F. SAUERWALD, *Z. anorg. Chem.*, 276 (1954) 155.
5 J. B. HEADBRIDGE, *Analyst.*, 83 (1958) 690.

RESEARCH ON THE ALLOYS OF NOBLE METALS WITH THE MORE ELECTROPOSITIVE ELEMENTS

II. MICROGRAPHIC AND ROENTGENOGRAPHIC EXAMINATION OF THE MAGNESIUM–PALLADIUM ALLOYS

RICCARDO FERRO

General Chemistry Institute and Physical Chemistry Laboratory of Genoa University, Genoa (Italy)

(Received December 18th, 1959)

INTRODUCTION AND METHODS OF STUDY

Information concerning the magnesium–palladium alloys is limited to some measurements of the variation of the lattice distances produced by adding small quantities of palladium to magnesium[1]. In the present paper a general outline is given of the system as a whole.

Preparation and general properties of the alloys

Preliminary tests have shown that the melting temperature of the alloys is relatively low, especially for the magnesium rich alloys, although it is higher for palladium rich alloys and probably reaches a maximum at a 1 : 1 composition (*ca.* 1400 - 1450°C). The method of preparation therefore consisted in placing the two metals (> 99.9% pure) in suitable proportions in an iron crucible (which was then sealed by means of electric welding) and successively heated in an electric furnace. The alloys having palladium contents of up to about 75 wt-% even when molten do not seem (at least not for short-time heating) either to wet or to dissolve iron readily: the maximum quantity of iron found in several samples was less than 0.2%. For alloys having a higher palladium content, it was necessary to avoid direct contact with the iron and, for this purpose, an alumina vessel placed inside the usual crucible was used. The various samples after having been heated (with stirring) to high temperature (1000 1400°C according to the presumed melting point) were then slowly cooled to 300°C (100–150 h) and then removed from the furnace. For alloys with a palladium percentage between 60–80% careful stirring was also necessary during the cooling to avoid inhomogeneous sedimentation caused by the different specific gravities and melting points of the several phases.

The alloys have a metallic luster and are not oxidised in the air, and those with less then 90% palladium are hard and, particularly between 30–70% palladium, very brittle. Generally they are rather compact with the exception of the ones between 75 85% palladium which, usually, are very porous.

The resistance to chemical attack increases with the palladium percentage. All the alloys are dissolved by aqua regia. Those with a low (20–30) palladium percentage

References p. 438

when treated with weak or very dilute acids leave a residue of palladium which is so finely divided as to have catalytic activity, for example, will ignite illuminating gas.

Chemical analysis

After solution of the alloy in aqua regia and evaporation to dryness with HCl, the palladium was precipitated with dimethylglyoxime, and the magnesium in the filtrate determined as pyrophosphate. The determination of palladium metal, by means of its precipitation as cyanide was also tried but this method was discarded because it gave slightly high results.

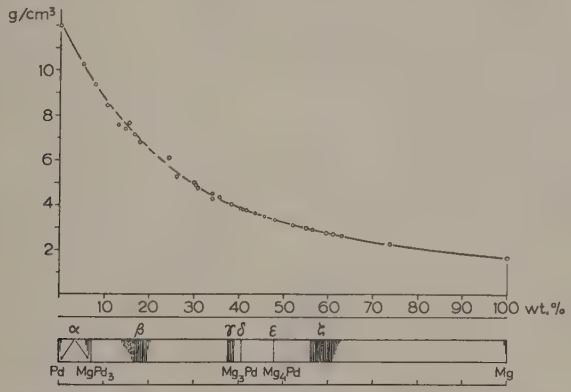

Fig. 1. Specific gravities (20–25°C) of Mg–Pd alloys. On the abscissas are approximatly indicated, as well as the Mg wt-%, the homogeneity ranges of the several phases.

Specific gravity determination

This was carried out by use of a pyknometer, which was filled with rectified benzene dried over sodium. The results are plotted in Fig. 1. The data on the alloys containing between 15–25% Mg are a little erratic owing to the porosity of the samples.

Micrographic examination

This was carried out, after dry polishing and etching with H_2O or HCl (diluted in relation to the increasing Pd percentage) in order to obtain separation between the phases present, or after etching with more or less diluted HNO_3 to show the grain boundaries.

X-ray examination

This was carried out on all the samples by the powder (Straumanis arrangement) method, using Cu Kα radiation and Fe Kα radiation for the magnesium-rich alloys, the photographs of which show a very high number of lines. For the palladium-rich alloys, to obtain measurable films it was necessary to anneal the filings of the samples for some hours at 500°C.

In some cases, as reported below, it was possible to obtain single crystals of the alloys.

References p. 438

TABLE I

MAGNESIUM–PALLADIUM ALLOYS

Alloy No.	*Mg % found*	*Pd % found*	*Stoichiom. ratio*	*Micrographic appearance*[a]	*Powder photograph appearance*
1	0.6	99.3	$MgPd_{37.7}$	Apparently homogeneous if normally cooled, but heterogeneous after annealing (2–3)	Reflexions of nearly pure Pd
2	5.63	94.98	$MgPd_{3.85}$		Pd + another c.f.c. phase
3	7.35	92.41	$MgPd_{2.86}$	Almost homogeneous (4)	In this region one set of c.f.c. reflexions only is observed always with the same constant
4	8.53	91.89	$MgPd_{2.45}$	Heterogeneous	
5	10.12	90.07	$MgPd_{2.03}$		
6	12.78	87.42	$MgPd_{1.56}$	Nearly homogeneous (5)	Reflexions of β phase
7	14.18	86.27	$MgPd_{1.39}$	No observations here owing to the poor characteristics of these alloys	Reflexions of β phase
8	15.22	85.43	$MgPd_{1.28}$		Reflexions of β' phase
9	16.27	83.86	$MgPd_{1.17}$		$\beta + \beta'$ reflexions
10	17.45	82.55	$MgPd_{1.08}$		β' reflexions
11	21.20	78.20	$Mg_{1.19}Pd$	Nearly homogeneous (6) with little of subsequent phase	Only the β phase reflexions are observable
12	23.94	76.28	$Mg_{1.38}Pd$	Always contain two phases: β and increasing quantities of γ (7–8)	In all this region only the γ phase reflexions are observable
13	25.78	74.15	$Mg_{1.53}Pd$		
14	29.70	70.30	$Mg_{1.85}Pd$		
15	30.00	70.6	$Mg_{1.86}Pd$		
16	30.56	69.30	$Mg_{1.93}Pd$		
17	31.22	68.65	$Mg_{2.00}Pd$		
18	32.28	67.52	$Mg_{2.10}Pd$		
19	33.87	66.06	$Mg_{2.25}Pd$		
20	35.90	63.48	$Mg_{2.48}Pd$	Almost homogeneous (9–10)	
21	36.18	63.67	$Mg_{2.49}Pd$		
22	38.27	61.73	$Mg_{2.72}Pd$	Homogeneous (11): γ	

TABLE I (Continued)

Alloy No.	*Mg % found*	*Pd % found*	*Stoichiom. ratio*	*Micrographic appearance*[a]	*Powder photograph appearance*
23	39.70	60.03	$Mg_{2.90}Pd$	Heterogeneous: two phases in nearly equal quantities (12)	γ and δ reflexions
24	40.03	59.39	$Mg_{2.96}Pd$	Nearly homogeneous with a small clearer part: γ (little) + δ	Only the δ phase reflexions are observable
25	40.60	59.05	$Mg_{3.02}Pd$		
26	41.34	58.33	$Mg_{3.11}Pd$	Nearly homogeneous with a small darker part (13): δ + ε (little)	
27	43.04	57.58	$Mg_{3.28}Pd$	Heterogeneous (14)	δ reflexions and very weak ε reflexions
28	43.35	57.33	$Mg_{3.32}Pd$		
29	45.60	55.11	$Mg_{3.63}Pd$		Only ε phase reflexions are observable
30	47.92	52.15	$Mg_{4.03}Pd$	Almost homogeneous with a small darker phase (15)	
31	48.47	51.84	$Mg_{4.10}Pd$		
32	49.61	50.66	$Mg_{4.30}Pd$	Two phases: ε with increasing quantities of ζ (16–18)	In this region only ζ phase reflexions are observable with increasing values of the lattice distances
33	51.84	48.09	$Mg_{4.73}Pd$		
34	54.79	45.33	$Mg_{5.30}Pd$		
35	56.24	43.76	$Mg_{5.64}Pd$	Homogeneous: ζ	
36	59.44	41.48	$Mg_{6.29}Pd$	Homogeneous (19): ζ	
37	60.75	39.13	$Mg_{6.81}Pd$	Almost homogeneous	
38	62.75	37.43	$Mg_{7.35}Pd$	Heterogeneous, with a small darker part (20)	
39	73.50	27.47	$Mg_{11.7}Pd$	Heterogeneous (21)	ζ phase + Mg reflexions

[a] The numbers of the corresponding microphotographs are quoted.

GENERAL VIEW OF THE SYSTEM AND OF THE EXISTING PHASES

The data obtained for the various alloys are shown in Table I. With the conditions of preparation described above one obtains a certain number of phases, some of which exist in a homogeneous range. The various phases are indicated with the letters α, β, etc., starting from the one having highest palladium content. (Only for the first alloy shown in the table, was it not possible to use the method of preparation described above. This was prepared by melting *in vacuo* (*ca.* 1550°C) from a Mg-richer alloy with a resultant loss of some magnesium by sublimation.)

From the table we deduce the existence of, at least, seven intermediary phases, *i.e.*:

α: a solid solution region extending at high temperatures from Pd up to *ca.* $MgPd_3$, which, on lowering of the temperature, breaks up into two phases: one nearly pure palladium and the other near to $MgPd_3$;

β and β': two solid state modifications in a homogeneous region around the composition corresponding to MgPd;

γ: a narrow region of solid solution with compositions around $Mg_{2.7}Pd$;

δ: corresponding to the Mg_3Pd compound;

ε: corresponding to the Mg_4Pd compound;

ζ: a remarkable region of solid solution around a composition such as Mg_6Pd.

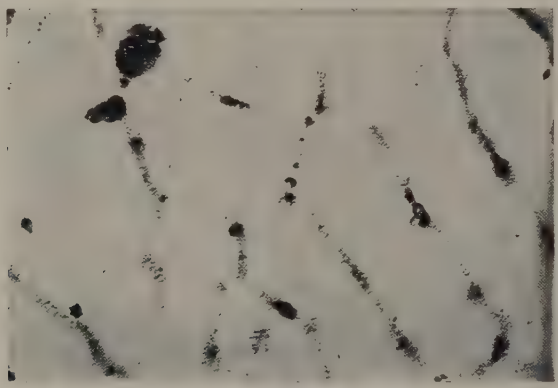

Fig. 2. 5.6$_3$% Mg, α phase, 200 ×.

DESCRIPTION OF THE VARIOUS PHASES

α phase. From the appearance of Figs. 2 and 3 (both of an alloy containing 5% Mg, the former drawn after regular cooling, the latter after 150 h annealing at 750°C) it appears that, in the palladium-rich part of the system, the alloys crystallise as a series of solid solutions, which, on lowering the temperature, split into two phases: one consisting of almost pure palladium and the other one having a composition near to $MgPd_3$ (see also Fig. 4 and the results of powder photographs).

The reflexions on the powder photograph of an alloy containing 7.4% Mg (almost homogeneous with and very close to 7.06% Mg, the theoretical composition for $MgPd_3$) agree with a face centered cubic lattice with $a_0 = 3.920$ Å*. The measured

* This value of the constant, as for the other substances, was obtained by a graphical method using the extrapolation function: $\frac{1}{2}(\cos\theta \cot\theta + \theta^{-1}\cos^2\theta)$.

References p. 438

specific gravity is 9.40 g/cm³: the value interpolated for $MgPd_3$ is *ca.* 9.58 from which we obtain the number $Z = 1.009$ of mol. $MgPd_3$ in the unit cell.

TABLE II

$MgPd_3$ POWDER PHOTOGRAPH SHOWING REFLEXION INTENSITIES Kα Cu RADIATION

h k l	$I_{calc.}$	$I_{obs.}$	*h k l*	$I_{calc.}$	$I_{obs.}$
111	11.9	ms	400	4.3	vw
200	7.5	m	331	22.5	s
220	9.1	m–ms	420	25.7	s
311	16.0	ms–s	422	59.2	vs
222	5.1	w			

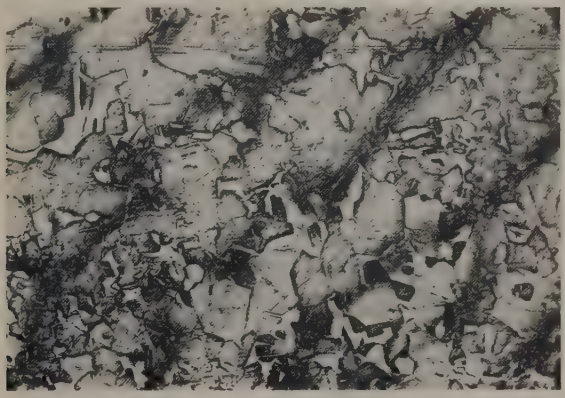

Fig. 3. The same as in Fig. 2 (after 150 h annealing at 750°C), 300 ×.

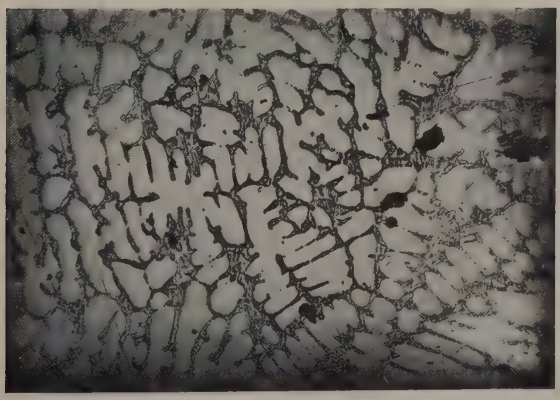

Fig. 4. 7.35% Mg (a little more than the theoretical composition for $MgPd_3$), 50 ×.

References p. 438

On the powder photograph of the 5% alloy there are two sets of reflexions agreeing with the existence of two cubic phases with sides $a_0 = 3.891$ Å (very close to the value of pure Pd) and $a_0 = 3.907$ Å (lower than that of $MgPd_3$ indicating partial miscibility). All the powders used for the X-ray examination were, as previously stated, annealed at 500°C. The calculated reflexion intensities reported in Table II (and compared with the observed values) were obtained on the assumption of a disordered structure. The X-ray data seem to exclude an ordered structure of the L_{12} type, since perceptible reflexions with mixed indices are not observed. However, perhaps this cannot be considered as a rigorous confirmation because, in any case, the intensities of these reflexions would be very low.

β phase. This phase is present in compositions near to MgPd. Its reflexions on powder photographs agree with the indices of a simple cubic lattice. As far as the value of the lattice constant is concerned, when measured on alloys containing 13–14% Mg (on which photographs only the β phase reflexions were observable), it was about

Fig. 5. 12.78% Mg, 100 ×.

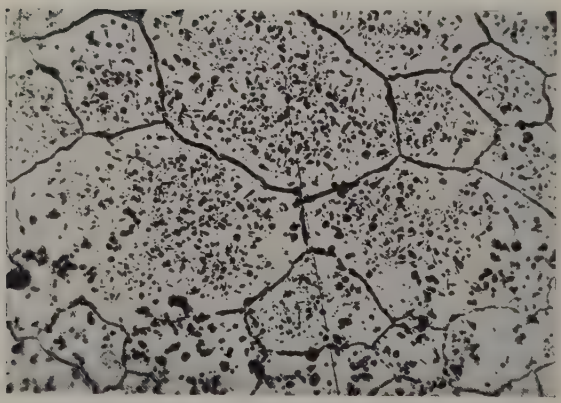

Fig. 6. 21.8% Mg, nearly pure β phase (note the segregation of the subsequent phase), 100 ×.

References p. 438

3.16 Å, whilst the value 3.17 Å was observed for alloys containing *ca.* 22% Mg (18.56% is the theoretical composition for MgPd). Under the conditions of preparation described above, the phase boundary can be estimated to be around 20–21% Mg on the magnesium side; however data concerning the boundary on the palladium side (*ca.* 14% at high temperatures?) are less certain, owing to the presence of another phase in this region (β', observed on the powder photographs).

To elucidate the structure of the β phase, an average value of the lattice constant and an experimental specific gravity of 6.8_5 interpolated for MgPd were used and it was shown that two atoms are present in the unit cell. In Table III are shown the observed intensities (photograph of an alloy with a slight excess of Mg over the theoric composition of MgPd) and those calculated for a CsCl structure. The agreement is not perfect: however, the hypothesis of a completely disordered disposition of atoms in the two positions 0, 0, 0 and $\frac{1}{2}$, $\frac{1}{2}$, $\frac{1}{2}$ may be excluded.

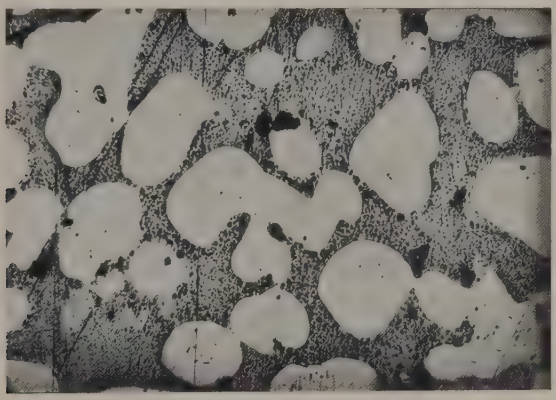

Fig. 7. 25.7_8% Mg, β (white) + γ, 50 ×.

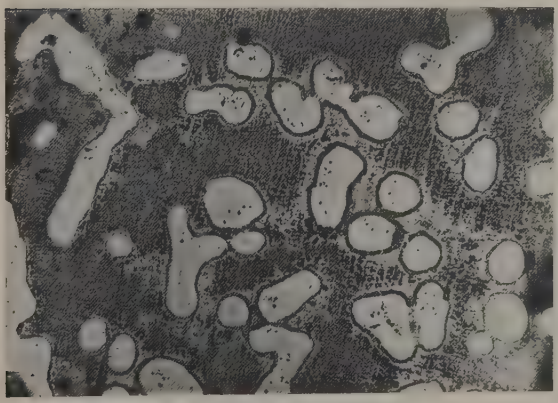

Fig. 8. 31.2_8% Mg, $\beta + \gamma$, 50 ×.

References p. 438

TABLE III

β PHASE POWDER PHOTOGRAPH SHOWING REFLEXION INTENSITIES, Kα Cu RADIATION

$h\,k\,l$	$I_{calc.}$	$I_{obs.}$	$h\,k\,l$	$I_{calc.}$	$I_{obs.}$
100	3.7	m–w	300 + 221	2.4	m
110	9.0	s	310	4.7	m
111	1.5	m–w	311	2.2	m–w
200	2.3	m–w	222	1.8	m–w
210	2.7	m	320	2.9	m–w
211	5.9	m–s	321	16.0	vs
220	2.3	m			

γ phase. This phase is homogeneous about a composition such as $Mg_{2.7}Pd$. The homogeneous region can be considered to stretch (at least with the above-mentioned conditions of preparation) between *ca.* 37 and 39% Mg (Figs. 9 to 12).

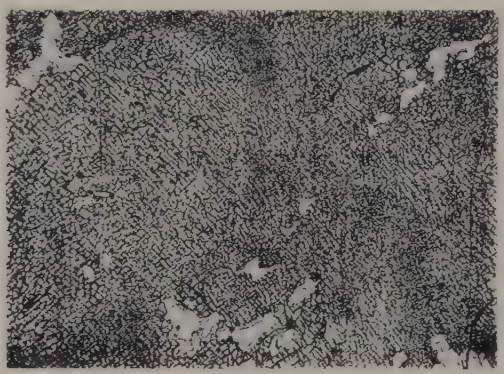

Fig. 9. 36.18% Mg, β (very little) + γ, 50 ×.

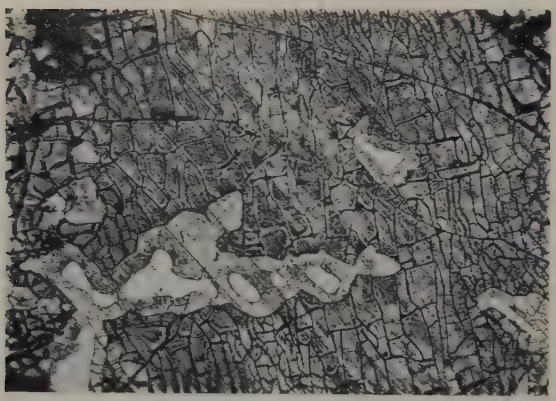

Fig. 10. The same as in Fig. 9 with higher magnification: 300 × (note the incomplete homogenisation of γ phase).

References p. 438

With this phase it was possible to obtain single crystals which showed a Laue symmetry D_{6h}. The best values for the constants, given below, have been obtained from the powder photographs using the method of least squares with corrected d's. From a homogeneous alloy with the composition 38.27% Mg and 61.73% Pd (corresponding to the formula $Mg_{2.72}Pd$) the following values were obtained:

$$a = 8.644 \text{ Å}, \quad c = 8.160 \text{ Å} \quad (c/a = 0.944)$$

From these values (using the experimental specific gravity $\varrho = 4.073$ g/cm³) we obtain $Z = 27.9$ (*ca.* 28) for the total number of atoms in the unit cell; the number of palladium atoms is (according to this composition) *ca.* 7.5. (For palladium richer alloys – already heterogeneous · the constants which presumably correspond to the saturation boundaries are:

$$a = 8.663 \text{ Å}, \quad c = 8.170 \text{ Å} \quad (c/a = 0.943)$$

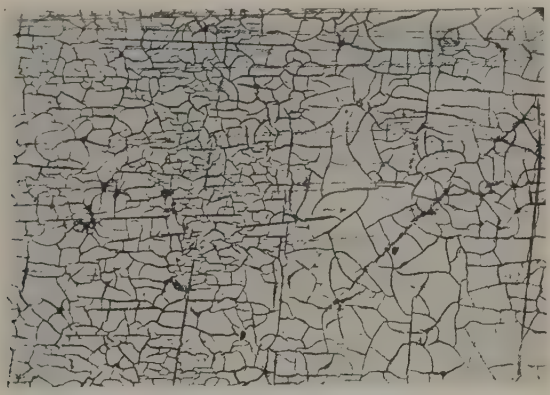

Fig. 11. 38.27% Mg, pure γ phase, 200 ×.

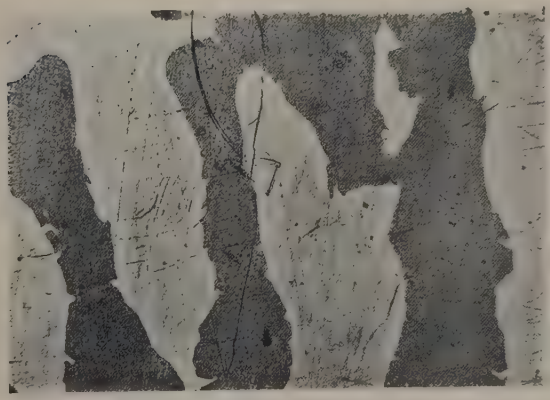

Fig. 12. 39.7% Mg, γ (white) + δ phase, 50 ×.

References p. 438

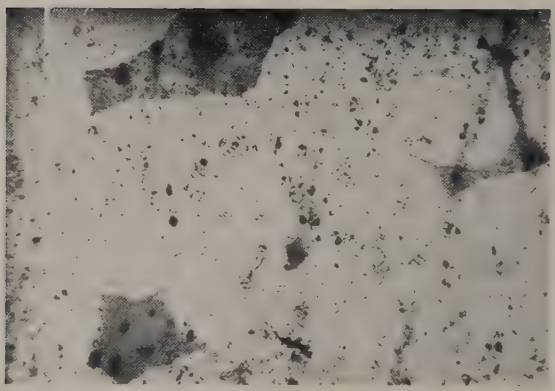

Fig. 13. 41.34% Mg, δ phase + little ε phase, 50 ×.

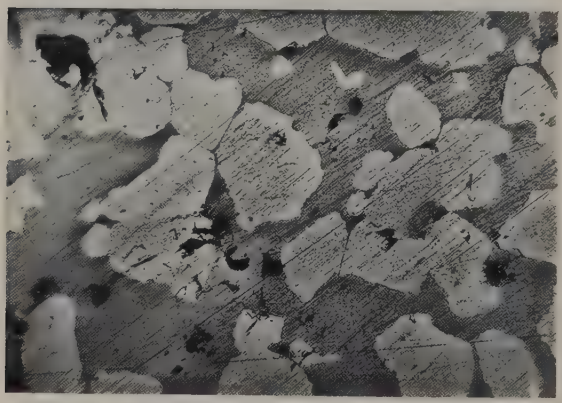

Fig. 14. 43.35% Mg, $\delta + \varepsilon$, 100 ×.

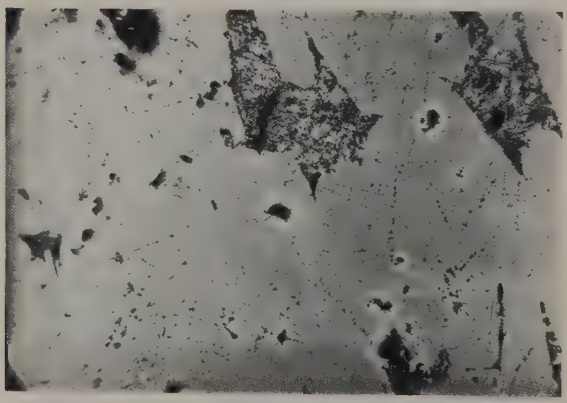

Fig. 15. 47.92% Mg, ε phase + little ζ phase, 100 ×.

From the Weissenberg photographs of the 0th, 1st, 2nd and 3rd lines around the hexagonal axis are obtained the following rules for the presence of the various reflexions: *hkil* for all orders, *hh2̄hl* only when $l = 2n$, *hh̄0l* for all the orders. The diffraction laws are therefore characteristic for the space groups D^4_{6h}, C^4_{6v} and D^4_{3h}. Perhaps, the structure of this phase may, on a first examination, appear similar to Al_5Co_2 (see ref.[2]) type, although for the theoretical composition of Mg_5Pd_2 (36.3% Mg) the alloys are still heterogeneous (see for example Fig. 9): it is possible, however, that complete homogeneity is reached only after very long periods of annealing (Fig. 10).

δ phase. This phase is homogeneous in agreement with the composition Mg_3Pd (theor. 40.61% Mg). The powder photographs for different compositions show no appreciable variation of the lattice distances.

Fig. 16. 49.61% Mg, ε (white) + ζ, 50 ×.

Fig. 17. 51.84% Mg, ε + ζ phases, 100 ×.

References p. 438

From the powder photograph it appears that this phase is isostructural with Mg_3Au (ref.[3]) (Na_3As type[4]) with constants:

$$a = 4.61_3 \text{ Å}, \quad c = 8.41_0 \text{ Å}, \quad c/a = 1.82_3 \quad \text{(hexagonal axes)}.$$

(From the experimental specific gravity $\varrho = 3.85_9$ g/cm^3, we obtain $Z = 8.02$ for the number of atoms in the unit cell.) As for the previous phase, the refinement of the crystal structure will be made on a later occasion.

ε phase. This phase may be considered as Mg_4Pd (theor. composition 47.69% Mg). From the microphotographs and the powder photographs (on which, for several compositions, no appreciable variation in the lattice distances can be observed) it appears that the range of homogeneity is very narrow.

The structure is unknown. The best value for the specific gravity of Mg_4Pd is presumably $\varrho = 3.43_2$ g/cm^3.

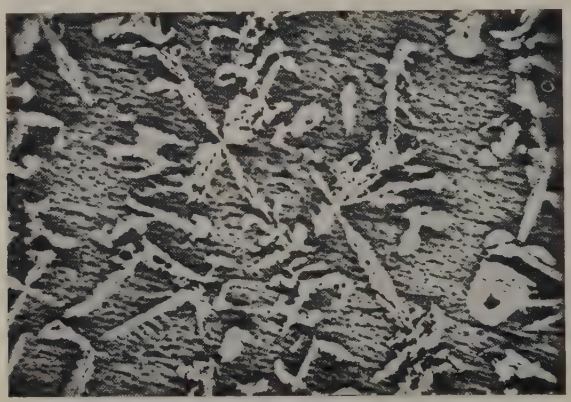

Fig. 18. 54.79% Mg, ε + ζ phases, 50 ×.

Fig. 19. 59.44% Mg, pure ζ phase, 200 ×.

References p. 438

ζ phase. The homogeneity range of this phase appears to be between *ca.* 56 and 61% Mg (that is between $Mg_{5.6}Pd$ and $Mg_{6.8}Pd$) at least from the appearance of alloys cooled down to 300°C (at a rate of 100°/day) and then removed from the furnace. Below are reported the values of the unit cell constants, for several compositions of this phase (which from the results of Laue photographs taken through some single crystals appears to be cubic) together with the number of atoms in the unit cells obtained from the experimental specific gravities:

Mg %	a_0 *(Å)*	ρ *(g/cm³)*	*Total number of atoms in the unit cell*	*Number of Pd in the cell*
56.24	20.060	3.011	398	60.0
59.44	20.145	2.864	394	54.7
60.75	20.182	2.804	398	51.0

It may be noticed however, that only from the appearance of the powder photographs could we obtain a larger range for the homogeneous region (at least towards

Fig. 20. 62.75% Mg, ζ phase + small amount of Mg, 100 ×.

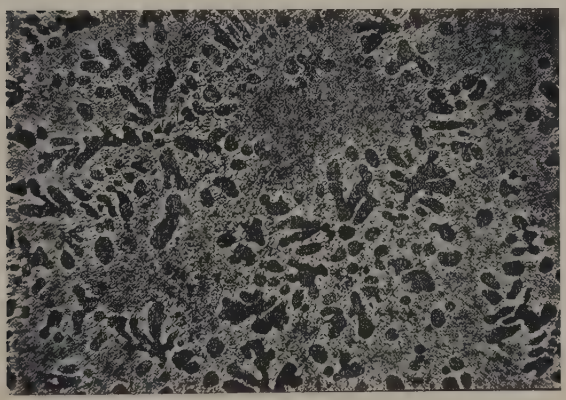

Fig. 21. 73.50% Mg, ζ phase + Mg (black), 100 ×.

References p. 438

higher Mg percentages): in fact, $a_0 = 20.21$ Å for a 62% Mg alloy, and for alloys at very high Mg contents reaches the value $a = 20.23$ Å.

With regard to the structure of this phase the conditions governing the presence of the indexes on the Weissenberg photographs are the following:

hkl only when $h + k = 2n$ and $k + l = 2n$ (*i.e.* face centered cubic)

Okl only when $k = 2n$, $l = 2n$
hhl only when $h + l = 2n$
hOO only when $h = 2n$

} that is excluding no other reflexions than those mentioned in the first condition.

The extinction laws are, therefore, those characteristic for the space groups: O_h^5, T_d^2 or O^3.

Moreover it seems possible that the cubic face centred lattice of this substance is very similar to a simple cubic one with $a' = a_0/2$. Actually the intensities of the permitted reflexions with $h + k + l = 2n + 1$ are generally much weaker than those with indexes $h + k + l = 2n$.

A Patterson projection on the unit cell face gave no easily interpreted results as, perhaps, could be expected from the high number of atoms in the unit cell in spite of the favourable ratio between the atomic scattering factors.

With the above-mentioned conditions of preparation the ζ phase is the last in the system since on the powder photographs of high Mg-rich alloys its reflexions appear mixed together with those of magnesium. The reflections of the latter, moreover, present very little variation compared with those of pure elementary magnesium. No further investigation of this point was made.

GENERAL REMARKS

A comparison between magnesium–palladium alloys and those of magnesium with the elements adjacent to palladium in the periodic system, (*i.e.* with rhodium and silver) might be valuable. As far as the magnesium–rhodium alloys are concerned, only one phase is known: MgRh[5], which is isostructural with the β phases of the magnesium–palladium and magnesium–silver systems.

The magnesium–silver system, on the contrary, is well known[6] and may be of interest because of the similarity (existing only in the silver-rich region) with the magnesium–palladium system *e.g.* the existence of the α and β phases, which in fact are isostructural.

ACKNOWLEDGEMENT

Much of the chemical analysis involved in this work was performed by Miss G. Rambaldi when she was working with a scholarship granted by the National Council of Nuclear Researches for the Solid State Physics Division of the Atomic Research Center of Ispra (Italy).

REFERENCES

1 R. S. Busk, *Trans. AIME*, 188 (1950) 1460.
2 A. J. Bradley and C. S. Cheng, *Z. Krist.*, 99 (1938) 480.
3 K. Schubert and K. Anderko, *Z. Metallk.*, 42 (1951) 321.
4 G. Brauer and E. Zintl, *Z. physik. Chem.*, B31 (1937) 323.
5 V. B. Compton, *Acta Cryst.*, 11 (1958) 446.
6 M. Hansen and K. Anderko, *Constitution of binary alloys*, McGraw-Hill Co., New York, 1958, p. 30.

POLISSAGE ÉLECTROLYTIQUE LOCAL (TECHNIQUE „ELLOPOL") POUR LA MÉTALLOGRAPHIE DU BÉRYLLIUM, DU ZIRCONIUM ET DU MOLYBDÈNE

PIERRE-A. JACQUET

Paris (France)

(Received December 23rd, 1959)

RÉSUMÉ

La nouvelle technique de polissage électrolytique local à l'aide d'un tampon („plug") jouant le rôle de cathode mobile et de réceptacle d'électrolyte présente de grands avantages sur les méthodes classiques utilisant la cellule simple ou les appareils semi-automatiques. Elle convient à la quasi totalité des matériaux métalliques et s'applique à toutes les formes et dimensions de spécimens ou de pièces.

Le présent article est limité aux conditions opératoires et à quelques résultats relatifs au béryllium, au zirconium, au zircaloy-2 et au molybdène. Il mentionne, d'autre part, d'une manière très succinte le procédé de réplique au vernis permettant la métallographie optique et électronique sur des objets volumineux ou de forme compliquée.

SUMMARY

A new technique of electrolytic local polishing using a plug which acts both as a mobile cathode and as a container for the electrolyte is described. This development provides great advantages compared with classical methods of electrolytic polishing which use a simple cell or semi-automatic apparatus, and it also suits nearly every metallic material, whatever the shape and dimensions of the specimen or part to be examined.

The present paper is limited to the operating conditions, and some results obtained, for beryllium, zirconium, zircaloy-2, and molybdenum. Brief reference is also made to the varnish replica technique for the examination of large or complicated samples by optical or electron microscopy.

INTRODUCTION

Le polissage électrolytique local a été mis au point en vue de résoudre l'important problème de la métallographie optique non destructive sur des objets qui, en raison de leur forme ou dimensions, ne peuvent être observés sur le microscope. L'élément de surface poli, et éventuellement attaqué, est recouvert d'un vernis nitrocellulosique spécial qui fournit après séchage une mince pellicule transparente portant l'empreinte fidèle de la topographie de l'original. Après décollement cette réplique est examinée soit directement par transmission, soit par réflexion et dans ce dernier cas il est avantageux de la métalliser par vaporisation sous vide d'un film d'aluminium ou d'or. Pour la micrographie électronique l'empreinte plastique sert de support à un film de carbone selon le procédé bien connu de BRADLEY.

Bibliographie p. 455

La technique de la métallographie optique et électronique non destructive a donné lieu à de multiples applications que l'on trouvera décrite en détail ailleurs[1,2,6].

L'expérience a montré, d'autre part, que le tampon électrolytique imaginé pour préparer la surface à l'endroit désiré sur l'objet, présentait dans le cas des petits échantillons métallographiques normaux des avantages considérables sur les méthodes habituelles utilisant la forme simple de la cellule ou les appareils semi-automatiques commerciaux. De plus, le tampon réalise également des processus anodiques d'oxydation et d'attaque nécessaires à la mise en évidence des caractéristiques de la microstructure indiscernables ou peu visibles sur la surface polie.

En définitive, le procédé connu maintenant sous le nom de technique ELLOPOL (electrolytic local polishing) est capable de résoudre d'une manière extrêmement simple tous les problèmes relatifs à la métallographie des matériaux métalliques.

Après un exposé d'ordre général, le présent article traite des conditions opératoires et de quelques résultats concernant le béryllium, le zirconium, le zircaloy-2 et le molybdène.

GENERALITES SUR LE POLISSAGE LOCAL

Sous sa forme primitive, proposée par J. MAZIA[3], le polissage électrolytique utilisant une cathode mobile ne pouvait concurrencer les autres méthodes de laboratoire. Outre qu'il ne s'appliquait qu'à un très petit nombre de matériaux, la qualité du poli était toujours insuffisante en raison d'attaques parasites.

La nécessité de disposer d'un moyen commode et efficace pour préparer de petits éléments de surface sur un objet trop volumineux pour être placé dans une cellule ordinaire ou sur un appareil du type DISA-ELECTROPOL, nous a conduit à perfectionner le „Brush Electropolishing" de MAZIA, tant en ce qui concerne la construction de la cathode mobile que la composition des électrolytes.

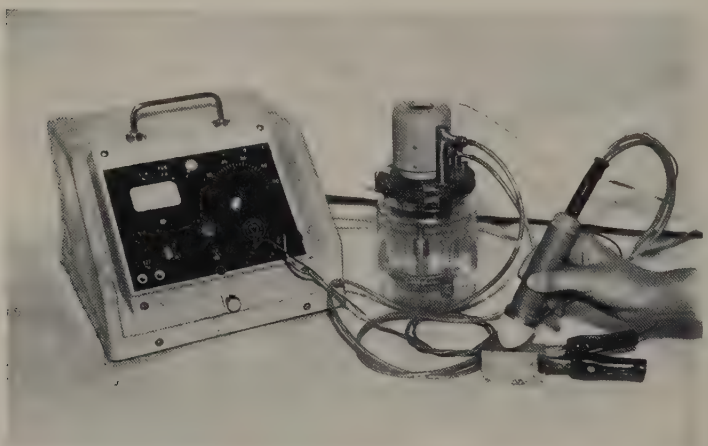

Fig. 1. Appareillage „ELLOPOL" pour le polissage, l'attaque et l'oxydation anodiques. Au centre le réservoir d'eau et la turbine assurant le refroidissement du tampon lorsqu'on ne dispose pas de canalisation d'eau.

Bibliographie p. 455

A la suite d'un très grand nombre d'essais systématiques nous sommes parvenus à mettre au point la technique dite ,,ELLOPOL'' qui par sa simplicité, sa souplesse et la qualité des résultats a déjà rendu de multiples services aux métallographes et est appelée, sans aucun doute, à se développer dans les laboratoires de recherches et de contrôles.

Les caractéristiques fondamentales de la technique ELLOPOL et ses avantages vis-à-vis des autres procédés connus à l'heure actuelle seront rapidement passés en revue avant de considérer les cas particuliers qui constituent l'objet essentiel de notre exposé.

Appareillage

L'appareil représenté Fig. 1 a été construit pour le travail au laboratoire, en atelier ou sur chantier. Il comprend un bloc d'alimentation, de réglage et de mesure des facteurs électriques branché sur le courant alternatif 120–240 V. Aux bornes de sortie sont connectés le tampon cathodique et le conducteur anodique assurant par un moyen approprié (pince, petit aimant permanent, etc...) le contact sur l'objet à polir.

Le tampon comporte un manche isolant et une tête en acier inoxydable refroidie intérieurement par un courant d'eau provenant d'une canalisation ou d'un réservoir muni d'une petite turbine. Sur la tête qui peut être de forme ogivale (modèle ,,OGIPOL'') ou pointue (modèle ,,SHARPOL'') s'adapte une coiffe amovible constituée de tissus en fibres artificielles inattaquables par les électrolytes et suffisamment spongieux pour en retenir une petite quantité.

Electrolytes

A de rares exceptions près les électrolytes classiques ne peuvent être utilisés avec le tampon. Les mélanges spéciaux sont des solutions diluées d'un acide minéral dans un ou plusieurs liquides minéraux ou organiques. Aucune de ces solutions ne présente de risque d'explosion et la seule précaution consiste à éviter de les manipuler à proximité d'une flamme.

Parmi ces nouveaux électrolytes, au nombre d'une douzaine et qui ont reçu des noms particuliers, il en est de polyvalents, c'est-à-dire capables de polir plusieurs types de matériaux. Inversement, un métal ou alliage donné peut parfois être poli avec deux ou même trois électrolytes de nature différente, et le choix dépend alors de diverses considérations relatives au résultat cherché, à la vitesse de dissolution, etc...

On a également mis au point des électrolytes capables de réaliser des processus anodiques d'oxydation ou d'attaque.

Conditions opératoires

Les facteurs les plus importants sont, d'une part la tension aux bornes dont la valeur réglée en circuit ouvert est généralement comprise entre 25 et 35 V, et d'autre part le mode d'application du tampon sur la surface. Cette application peut se faire: (a) par touches successives, c'est-à-dire alternances de contact de durée variable (depuis une fraction de seconde jusqu'à 7 à 10 sec) et d'interruption (de l'ordre de 1 à 3 sec); (b) par déplacement à vitesse convenable selon un mouvement giratoire ou rectiligne. La première modalité restreint l'effet de polissage à la zone d'impact

Bibliographie p. 455

(environ 0.5 cm^2 avec le modèle SHARPOL et 1 cm^2 avec le modèle OGIPOL) tandis que la seconde permet éventuellement de l'étendre autant qu'on le désire. Le polissage de grandes superficies peut se faire aussi en appliquant non plus l'extrêmité de la coiffe, mais une fraction de sa surface latérale qui est roulée de part et d'autre d'une position moyenne.

Outre les conditions d'application qui définissent dans une certaine mesure l'homogénéité ou, au contraire, la sélectivité de la dissolution, le résultat dépend aussi du volume de liquide retenu dans la coiffe et surtout de la pression de contact exercée. Un gros excès d'électrolyte sur la surface est en général à éviter et le tampon doit toujours être manipulé d'une „main légère", une pression exagérée provoquant sur le métal l'empreinte de la trame du tissu externe.

Dans la plupart des cas l'intensité reste comprise entre 0.1 et 0.3 A, descendant parfois jusqu'à 0.05 A. Une trop forte valeur d'intensité est la conséquence d'un échauffement anormal, surtout à craindre avec les échantillons de petite taille et les tôles minces. Pour de tels objets les conditions de refroidissement sont beaucoup améliorées en les posant sur un bloc massif de métal bon conducteur, ce qui facilité également la prise du contact électrique.

La durée d'une opération de polissage dépend à la fois de l'état initial (il est rarement nécessaire de pousser la préparation mécanique au-delà du papier potée émeri OO paraffiné) et de la vitesse de dissolution anodique qui peut varier entre 2 et 15 microns/min selon le matériau et l'électrolyte. Lorsque, pour une raison quelconque, l'électrolyse doit être poursuivie longtemps, il est recommandé d'opérer en plusieurs stades de durée moyenne 2 à 3 min séparés par un lavage et un séchage de la surface.

Bien que le mode opératoire dont on vient de décrire les grandes lignes paraîsse comporter une large part d'empirisme, l'expérience prouve que la pratique en est aisée à acquérir. D'ailleurs, à moins de s'écarter beaucoup des conditions optimales, il est exceptionnel que le résultat soit franchement mauvais. De plus, l'opérateur ayant toujours sous les yeux la surface de l'objet se rend compte immédiatement de l'effet macroscopique de tel ou tel facteur.

En ce qui concerne les conditions générales des processus d'oxydation et d'attaque anodiques susceptibles d'être réalisés avec le tampon, nous renvoyons le lecteur à nos publications antérieures[4,13].

Avantages de la technique ELLOPOL

Ils peuvent se résumer de la façon suivante:

1. Possibilité de réaliser non seulement le polissage, mais encore tous les processus anodiques qui exigent d'habitude une cellule dont les inconvénients sont bien connus. Ces processus comprennent l'oxydation et les attaques micrographiques, l'obtention de répliques d'alumine pour la microscopie électronique des métaux légers, le décollement de ces répliques et aussi des répliques de carbon sur métaux quelconques.

2. Aucune limitation quant à la forme et aux dimensions de l'objet. Cet avantage, qui permet la métallographie non destructive par répliques, subsiste en métallographie classique, car on évite le découpage d'un spécimen trop volumineux pour être immergé dans une cellule ou de forme non adaptée au polissage sur appareil semi-automatique.

Bibliographie p. 455

3. La surface restant sous ses yeux, l'opérateur peut suivre les progrès du polissage ou de l'attaque.

4. La consommation d'électrolyte est très minime, et celui-ci étant renouvelé conserve sa composition initiale d'une opération à une autre.

5. Du fait de la faible valeur de la densité de courant la vitesse de dissolution est lente, ce qui permet: (a) le polissage de feuilles très minces (0.01 mm par exemple); (b) l'étude des couches très superficielles (à partir de 2 microns); (c) de réduire au minimum le phénomène gênant de la dissolution préférentielle des arêtes.

6. La périphérie de la zone polie n'est marquée par aucune dénivellation brutale. Cette caractéristique est importante lorsqu'il s'agit d'examiner des pièces qui doivent être mises ensuite en service.

GENERALITES SUR LA METHODE DE REPLIQUES

D'emploi général pour la micrographie électronique, les répliques sont ignorées en métallographie optique. En effet, elles sont spécialement intéressantes dans les cas ou l'examen direct est impossible, ce qui suppose une méthode de préparation de la surface, et aussi un procédé de réplique simple, applicable à des superficies étendues et de forme quelconque. Le polissage au tampon réalise maintenant la première condition, mais aucun des divers produits d'empreinte connus ne répond vraiment à la seconde.

C'est à VAN EFFENTERRE que revient le mérite d'avoir mis au point une technique de réplique susceptible de résoudre tous les problèmes de la métallographie non destructive, aussi bien dans le domaine optique que dans celui du microscope électronique. Les perfectionnements successifs concernant l'élaboration, le montage et l'observation de ces répliques ont fait l'objet de plusieurs publications[1] et nous n'en donnerons ici qu'un très bref aperçu.

Le produit sélectionné est un vernis nitrocellulosique liquide qui est étendu par gravité ou à l'aide d'un pinceau. Après séchage à l'atmosphère ordinaire, ou mieux sous un rayonnement infra rouge, la pellicule est décollée soit à sec, soit après contact plus ou moins prolongé avec une solution diluée de mouillant (teepol par exemple) lorsqu'une trop forte adhérence risquerait de provoquer des arrachements.

L'observation optique de la topographie reproduite sur le plastique peut se faire en lumière transmise (projecteur de profil, lanterne de projection, microscope droit, etc...) ou en lumière réfléchie sur le microscope métallographique. Le premier moyen donne d'excellents résultats pour la macrographie, tandis que le second est préféré dès que le grossissement dépasse une centaine de diamètres. La netteté, et surtout le contraste des images obtenues avec la lumière réfléchie, sont considérablement améliorés si l'empreinte est métallisée par vaporisation sous vide d'aluminium ou d'or.

Les examens comparatifs sur surfaces originales et sur leurs répliques au vernis prouvent la fidélité de reproduction des plus fins détails. Pour passer au domaine du microscope électronique il suffit d'appliquer la technique de BRADLEY[5], c'est-à-dire que l'empreinte est recouverte d'une mince film de carbone vaporisé, dont les fragments sont recueillis après dissolution du plastique dans un solvant approprié.

Il est important de préciser que cette technique qui convient à des surfaces de profil très tourmenté a pu être appliquée récemment à tous les types de cassures (fractographie et microfractographie non destructives[6]).

Bibliographie p. 455

APPLICATIONS METALLOGRAPHIQUES

Dans son état présent le polissage au tampon s'applique aux matériaux suivants: aluminium et ses alliages (y compris les alliages de fonderie riches en silicium et les produits frittés ,,Sap''), béryllium, cadmium, chrome, cuivre et ses alliages mono et polyphasés (laitons, bronzes à toutes teneurs en étain, cupro-aluminiums, cupro-nickels, etc...) fer, aciers au carbone, aciers alliés, fontes, aciers inoxydables ferritiques et austénitiques, aciers à coupe rapide riches en tungstène, magnésium et ses alliages, molybdène, nickel, cobalt, alliages spéciaux (vitalium, mumétal, nimonics de toutes nuances), plomb, étain, titane et ses alliages, uranium et ses alliages, zinc, zirconium et zircaloys.

Parmi ces matériaux nous avons choisi le béryllium, le zirconium, le zircaloy-2 et le molybdène pour fournir des exemples précis des conditions opératoires et illustrer la qualité des résultats obtenus.

Béryllium

Du point de vue de la métallographie du béryllium deux caractères importants du métal doivent être considérés. D'une part sa toxicité lorsqu'il est à l'état de fines particules, d'autre part sa grande sensibilité à l'écrouissage. On devra donc s'efforcer de supprimer, ou tout au moins de réduire au strict minimum, les opérations mécaniques de découpage, de dégrossissage aux outils et d'abrasion sur les papiers émeri. A ce point de vue la métallographie non destructive par polissage local et réplique est particulièrement avantageuse pour les laboratoires qui ne disposent pas de moyens de protection contre le danger des poussières.

Le meilleur polissage est obtenu avec l'électrolyte dénommé ,,BEPER''* sous une tension à vide de l'ordre de 45 V. La coiffe du tampon imbibée de la quantité de solution juste nécessaire pour qu'une goutte se dépose au point d'impact est appliquée d'abord par quelques touches, selon une cadence très rapide, puis déplacée d'un mouvement giratoire assez lent sans appuyer sur la surface. L'intensité du courant ne doit pas dépasser 0.10 à 0.15 ampère si le refroidissement est effectué correctement.

La vitesse de dissolution est de l'ordre de 2 à 2.5 microns par min. Par conséquent, si l'état de surface microgéométrique initial n'est pas très bon, ou bien si l'on désire, pour une raison quelconque, éliminer une épaisseur notable de métal, la durée d'électrolyse peut atteindre, et même dépasser, une dizaine de minutes.

Dans ces conditions, et surtout si l'échantillon est de petite taille, un certain échauffement peut se produire et entraîner une très légère attaque que l'on fait disparaître en procédant à un deuxième stade de durée limitée à 2 min environ, la surface étant, bien entendu, lavée et séchée, entre les deux opérations. Un effet d'attaque tend aussi à se manifester lorsque le tampon au lieu d'être déplacé par rotation est appliqué continuellement par touches à cadence rapide.

Cette technique de polissage a été employée pour étudier la microstructure de divers spécimens de béryllium.

La Fig. 2, relative à une plaque fortement oxydée pendant le laminage à chaud, prouve que le polissage est possible sans préparation mécanique de la surface et, de

* Cet électrolyte convient également au polissage de l'aluminium, du magnésium, du cadmium et de leurs alliages respectifs.

Bibliographie p. 455

ce fait, les grains sont privés des macles qui se seraient produites si la croûte épaisse et rugueuse d'oxyde noir avait été retirée par abrasion ou rectification.

La Fig. 3 montre deux aspects des impuretés dans une plaquette de béryllium

Fig. 2. Béryllium laminé à chaud. La croûte épaisse et rugueuse d'oxyde est enlevée par un polissage de 6 mn. La sous-structure visible sur certains grains correspond sans doute à la diffusion de l'oxygène dans le réseau. Photographie en lumière polarisée (× 400).

„Hot pressed"*: des cordons noirs formés vraisemblablement d'oxyde, localisés sur les contours des grains, et de petits éléments de couleur brune plus dispersés.

Un autre exemple concerne une plaquette „Hot pressed and sintered"* qui présentait de nombreuses piqûres produites par un polissage chimique initial. Bien que ces

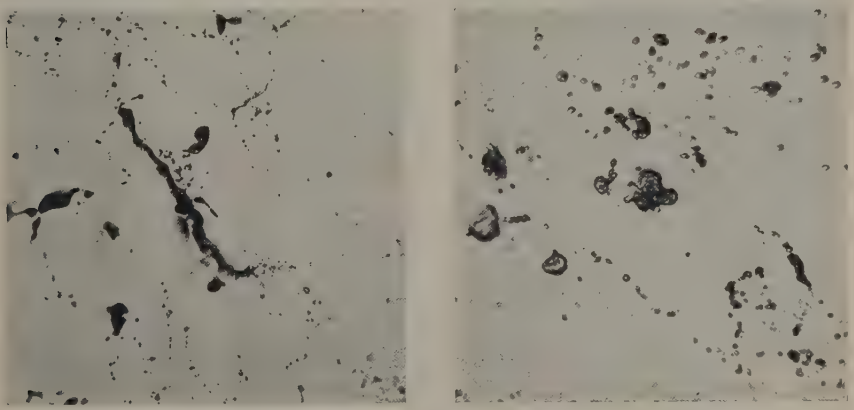

Fig. 3. Béryllium „Brush Hot Pressed". Polissage 8 minutes. a, × 400. b, × 1000.

* Cet échantillon nous a été aimablement fourni par M. R. J. KING, de The English Electric Company Ltd., que nous tenons à remercier ici.

Bibliographie p. 455

défauts ne soient que partiellement éliminés par un polissage au tampon de 6 min, les filaments d'oxyde typiques sont nettement révèlés (Fig. 4).

Des caractéristiques structurales intéressantes ont été observées sur un spécimen

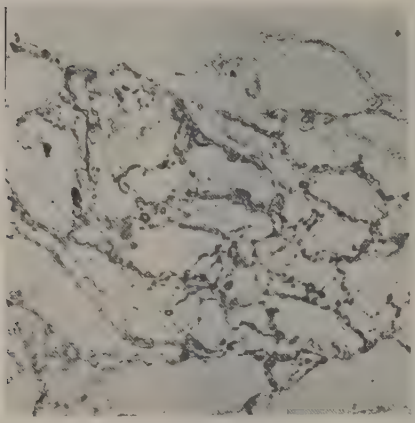

Fig. 4. Béryllium „Péchiney Hot Pressed and Sintered". Polissage 6 minutes (× 1000).

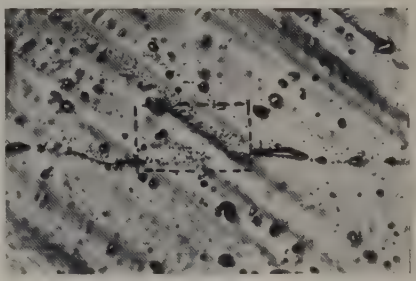

Fig. 5. Béryllium „Imperial Smelting Co, Vacuum Cast". Surface rectifiée à l'outil. Polissage 9 minutes (dissolution environ 20 microns). La ligne horizontale à mi-hauteur est un joint intergranulaire. Les traces de rayures d'outil sont encore visibles (× 160).

de béryllium fondu sous vide* dont la surface avait subi une fine rectification mécanique. Les perturbations provoquées par l'outil sont si intenses qu'une épaisseur d'environ 10 microns doit être retirée avant que les grains ne deviennent visibles sous l'éclairage en lumière polarisée. Les couches superficielles mises à nu par le polissage

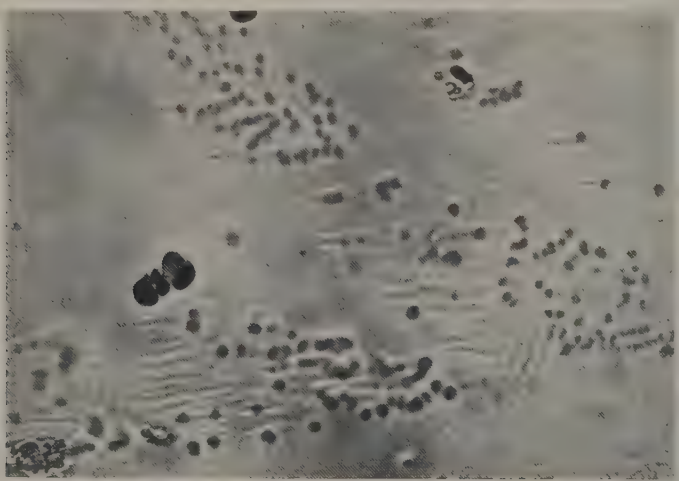

Fig. 6. Région encadrée sur la Fig. 5. Micropiqûres en relation avec la déformation plastique (× 1000).

* Cet échantillon nous a été aimablement fourni par M. R. J. King, de The English Electric Company Ltd., que nous tenons à remercier ici.

Bibliographie p. 455

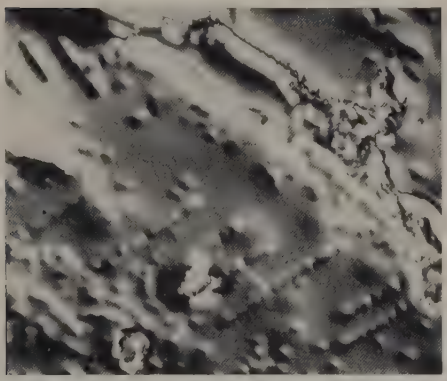

Fig. 7. Même surface que Fig. 5. Séquences de micropiqûres au voisinage d'un joint intergranulaire. Remarquer la courbure d'une séquence autour d'une inclusion. Photographie en contraste interférentiel à deux ondes polarisées (× 1000).

(a) (b)

Fig. 8. Même surface que Fig. 5 après un nouveau polissage de 2 min (dissolution supplémentaire environ 5 microns). (a) Alignements transgranulaires de micropiqûres. Les flèches montrent la frontière du grain contenant des inclusions d'oxyde (× 400). (b) Même champ photographié en lumière polarisée. Les micropiqûres se placent le long d'un seul des deux joints des diverses macles (× 500).

dans des conditions qui favorisent une légère attaque (cadence rapide du tampon) contiennent un nombre considérable de micropiqûres. Le nombre de ces points d'attaque privilégiée diminue à mesure que le plan considéré s'éloigne de la surface, et ils tendent à se localiser sur des domaines en relation manifeste avec les traces des rayures produites par l'outil (Figs. 5 et 6.)

Des dispositions régulières, comme les séquences montrées (Fig. 7), suggèrent que les micropiqûres se forment à l'émergence de dislocations. Des ponctuations de ce genre sont observées aussi le long de certaines macles mécaniques, mais il est remarquable qu'une seule des deux frontières de telle macle se trouve ainsi attaquée (Fig. 8)*. En suivant l'évolution d'un même champ après un nouveau polissage on constate que les micropiqûres produites au stade antérieur tendent à s'estomper et qu'il s'en forme d'autres qui coïncident toujours très exactement avec la nouvelle position de la frontière de la macle considérée (Fig. 9). Ceci prouve qu'il ne peut pas s'agir d'hétérogénéités chimiques, oxyde par exemple, réparties au hasard dans les grains. En revanche, le phénomène correspondrait bien à l'attaque sélective d'une ligne de dislocations émergeant à la surface sous un angle différent de 90°.

Ces observations montrent l'intérêt de la technique du polissage ELLOPOL

(a) (b)

Fig. 9. Même surface que Fig. 8 après un nouveau polissage de 2 min (dissolution supplémentaire environ 5 microns). (a) Région encadrée sur la Fig. 8a. On voit simultanément les traces des anciennes micropiqûres (larges taches claires) et les nouvelles, considérablement plus fines. Photographie en contraste interférentiel (× 1600). (b) Champ de a (un peu moins étendu vers le bas et un peu plus étendu vers le haut). Photographie en lumière polarisée (× 1600).

* Un phénomène analogue a été signalé dans le cas des macles du zinc[7].

Bibliographie p. 455

pour étudier la déformation plastique du béryllium. Les processus qui accompagnent le travail de la surface à l'outil n'étant pas simples (l'action mécanique par elle-même complexe est accompagnée d'effets thermiques), les expériences devraient porter sur des éprouvettes préparées spécialement, ainsi que l'a fait GILMAN dans le cas du zinc[7]. Pour des recherches de ce genre, la tente vitesse de dissolution est un précieux avantage du tampon que ne possèdent pas les autres procédés de polissage électrolytique faisant intervenir des densités de courant considérablement plus élevées[8].

L'application au béryllium de la technique de répliques au vernis est limitée actuellement à l'examen des aspects visibles en lumière normale. En effet, l'anisotropie optique qui permet de distinguer la cristallisation de la surface polie observée entre nicols croisés n'est pas reproduite par l'empreinte plastique. On connaît cependant un moyen susceptible de créer une anisotropie artificielle conditionnée par le microprofil de la surface et, par conséquent, transposable sur la réplique. Il suffit de soumettre la surface polie à une attaque produisant sur les plans cristallographiques un réseau continu de figures de corrosion d'extrême finesse. Cet artifice a été appliqué avec succès à des métaux isotropes (aluminium et ses alliages, cuivre, aciers austénitiques)[9] et anisotropes (étain, uranium-α)[10], mais pour le béryllium nous n'avons pas réussi encore à définir les conditions d'attaque satisfaisantes.

Zirconium et Zircaloy-2

Deux électrolytes ont été sélectionnés: le „BUPER" qui contient les mêmes éléments que le „BEPER", mais dans des proportions différentes, et le „PEROC", qui convient d'ailleurs aussi à certains alliages d'uranium.

TABLEAU I

POLISSAGE DU ZIRCONIUM ET DU ZIRCALOY-2

Electrolyte	*Tension à vide*	*Conditions d'application du tampon*	*Vitesse de dissolution microns/min*
BUPER	45 à 50	Touches à cadence d'abord rapide puis plus lente	3
BUPER	40	Déplacement rectiligne	4
PEROC	20	Déplacement rectiligne assez rapide	15 à 18

Utilisés dans les conditions résumées au Tableau I, les deux électrolytes donnent sensiblement les mêmes résultats sur le zirconium. Toutefois le BUPER sera préféré pour réduire au minimum l'attaque des microconstituants, car la densité de courant étant très faible les risques d'échauffement sont moindres qu'avec le PEROC. Ce dernier a l'avantage d'une grande vitesse de dissolution, d'où un polissage très rapide (20 à 30 sec).

Les Figs. 10 et 11 donnent des exemples de la qualité du poli obtenu à partir de spécimens abrasés jusqu'au papier potée émeri OO paraffiné. On remarque l'absence de tout effet de relief des microconstituants et de gravage de la matrice. Les surfaces ainsi obtenues sont très réactives à la lumière polarisée, même sous les forts grossissements (Fig. 12).

Bibliographie p. 455

Contrairement au zirconium l'alliage zircaloy-2 s'est montré sensible à la nature de l'électrolyte de polissage. Alors que pour certains échantillons le „BUPER" et le „PEROC" fournissent pratiquement le même aspect micrographique (Fig. 13), d'autres subissent avec le PEROC une attaque sélective qui n'apparaît pas dans le cas du BUPER (Fig. 14). Il est important de souligner que tous les spécimens prélevés dans les billettes forgées à partir de lingot de zircaloy-2 fondus sous vide se compor-

Fig. 10. Zirconium forgé. Polissage de 3 min mettant en évidence les microprécipités de carbure (× 500).

Fig. 11. Zirconium déhafnié d'origine U.S.A. Plaquettes d'aspect cristallin révélées par un polissage de 2 min (× 1000).

Fig. 12. Même surface que Fig. 10. Photographie en lumière polarisée. Remarquer l'excellente définition des microprécipités de carbure (× 1600).

Bibliographie p. 455

tent comme l'échantillon de la Fig. 13, tandis que la différence des aspects a et b de la Fig. 14 caractérise tous les spécimens provenant du forgeage de lingots du même alliage fondu en atmosphère d'argon. On remarque, d'autre part, que la microstructure du type Fig. 14 contient des éléments d'hétérogénéités de forme filamenteuse à peine révèlés par le polissage ,,BUPER'' et qui deviennent beaucoup plus apparents

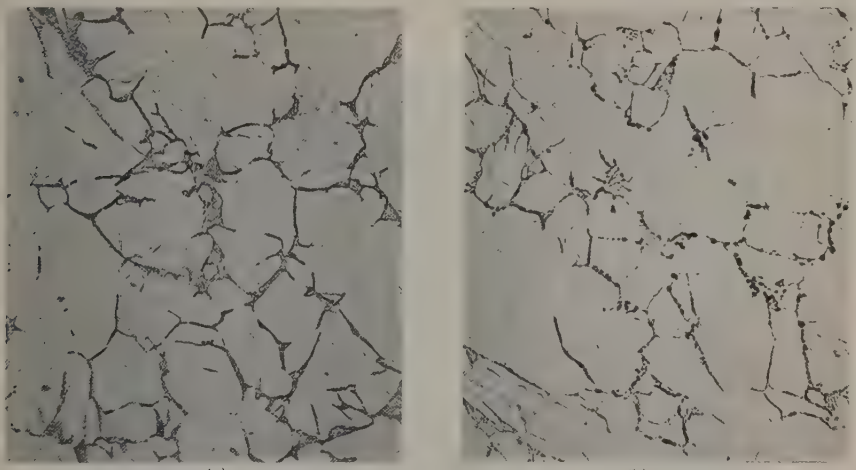

(a) (b)

Fig. 13. Billette de zircaloy-2 forgée à partir d'un lingot fondu sous vide (× 400). (a) Polissage de 2 mn avec l'électrolyte ,,BUPER''. (b) Polissage de 2 mn avec l'électrolyte ,,PEROC''.

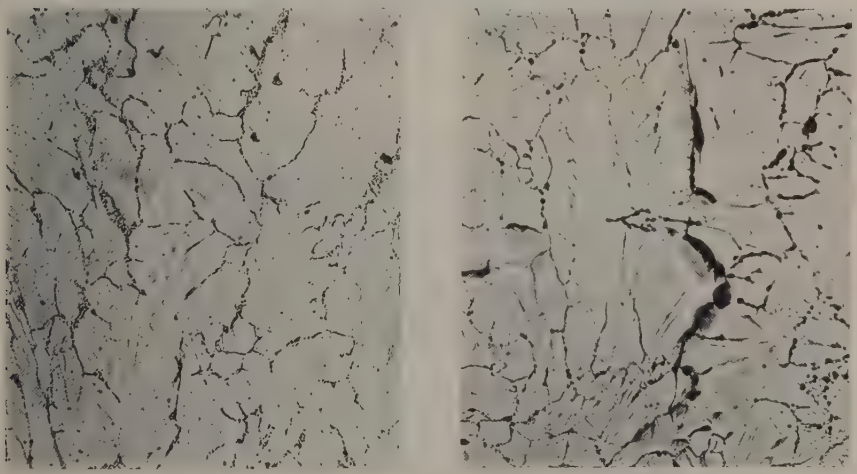

(a) (b)

Fig. 14. Billette de zircaloy-2 forgée à partir d'un lingot fondu en atmosphère d'argon (× 400). (a) Polissage de 2 mn avec l'électrolyte ,,BUPER''. (b) Polissage de 30 sec avec l'électrolyte ,,PEROC''.

Bibliographie p. 455

après l'oxydation anodique dans les conditions décrites plus loin (Fig. 15). L'expérience indique que ce sont précisément ces éléments filamenteux qui subissent l'attaque sélective pendant le polissage avec l'électrolyte „PEROC".

Ces résultats, et d'autres encore, seront discutés ailleurs. Précisons toutefois qu'ils nous paraîssent susceptibles de contribuer à éclaircir le problème encore controversé de la nature des défauts du zircaloy-2, connus sous le nom de „structural stringers" (voir par ex. réf.[11]). En tout cas, pour des études de ce genre, la technique du tampon

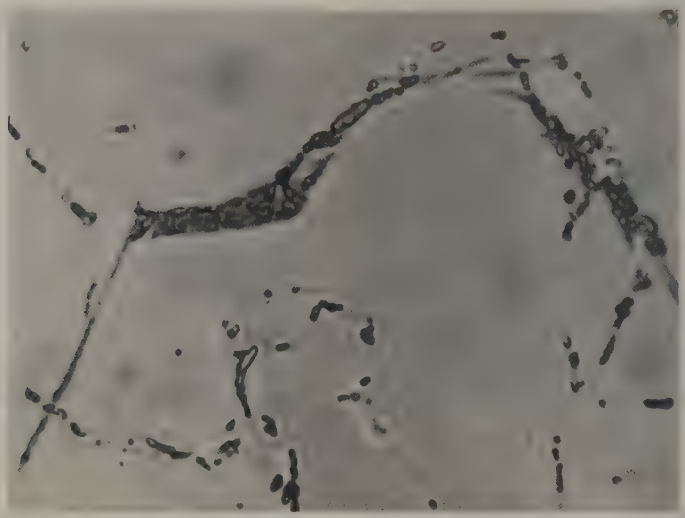

Fig. 15. Billette de zircaloy-2 forgée à partir d'un lingot fondu en atmosphère d'argon. Polissage 3 mn avec l'électrolyte „BUPER" suivi d'oxydation anodique avec l'électrolyte OPALU, 30 sec sous 10 V, puis 30 sec sous 20 V (× 2500).

électrolytique se montre bien supérieure aux méthodes classiques de polissage mécanique ou de polissage chimique: la première introduit des perturbations considérables, et la seconde provoque des phénomènes d'attaque parasite incompatible avec l'observation précise des plus minimes hétérogénéités.

De même que pour le béryllium, nous avons pu mettre en évidence l'existence de microdomaines à haute réactivité chimique dans les couches superficielles du zircaloy-2 soumis à un travail mécanique. Ici les points d'attaque sont très souvent alignés sur des lignes courbes et leur relation avec l'émergence des dislocations semble incontestable (Fig. 16).

Le tampon ELLOPOL réalise aisément l'oxydation anodique préconisée par PICKLESIMER pour la métallographie du zirconium[12]. La solution complexe employée par cet auteur est remplacée par l'électrolyte dénommé „OPALU" mis au point en vue de l'oxydation anodique de l'aluminium et des alliages légers[13]*.

Les conditions opératoires ne sont pas critiques. L'intensité initiale qui s'établit au

* L'électrolyte OPALU présente aussi de remarquables propriétés pour le polissage au tampon de l'uranium pur et allié, principalement lorsqu'il s'agit de polir de grandes surfaces[14].

Bibliographie p. 455

premier contact du tampon est d'autant plus élevée que la tension aux bornes est elle-même plus grande, mais quelle que soit cette tension (dans les limites 5 à 50 V) l'intensité devient quasi nulle au bout de quelques secondes. Le film d'oxyde prend d'abord une coloration générale bleu-violacé, d'intensité variable sur les différents grains du métal, puis devient jaune d'or sous une tension plus forte. A ce stade les grains ne sont plus différenciés, alors qu'au contraire les phases étrangères éventuellement présente acquièrent des teintes spécifiques.

Fig. 16. Billette de zircaloy-2 forgée à partir d'un lingot fondu en atmosphère d'argon. La surface rectifiée à l'outil est abrasée aux papiers émeri à sec, puis sous l'eau, polie 90 sec avec l'électrolyte BUPER et enfin soumise à des touches rapides du tampon pendant 20 sec (× 2500).

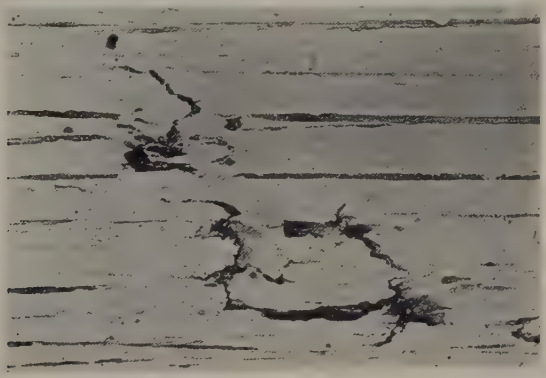

Fig. 17. Surface d'une tôle laminée à partir de la billette présentant la microstructure Fig. 14. Photographie en lumière réfléchie de la réplique, montrant les défauts du genre „stringers" (× 160).

Bibliographie p. 455

Le zircaloy-2 se comporte un peu différemment: le film bleu–violacé apparaît quand la tension est comprise entre 20 et 30 V, puis se décolore sous 40 V. Ainsi qu'on l'a vu plus haut ce procédé est intéressant pour détecter les hétérogénéités du type „filamenteux". Sous les plus forts grossissements optiques ces filaments montrent alors une sous-structure (Fig. 15) que nous tentons actuellement de résoudre avec le microscope électronique.

Dans son état actuel la métallographie non destructive du zirconium et de ses alliages présente la limitation déjà signalée à propos du béryllium, car l'on n'a pas trouvé de technique d'attaque capable de créer l'anisotropie artificielle transposable sur l'empreinte plastique, et indispensable aux observations en lumière polarisée. En revanche, il est possible de contrôler, avec une réplique au vernis, les hétérogénéités structurales d'un lingot, d'une billette ou d'une tôle aux endroits préparés à l'aide du tampon ELLOPOL. Dans le cas des tôles, une réplique prise directement reproduit les défauts de surface éventuels; ainsi, la Fig. 17 montre les fissures du genre „stringers" sur la surface d'une tôle obtenue par laminage de la billette forgée possédant la structure visible Fig. 14.

Molybdène

Un excellent polissage est obtenu avec l'électrolyte spécial „MESUL" sous une tension à vide comprise entre 20 et 30 V. Le tampon est appliqué par touches à cadence rapide pendant quelques secondes, puis avec des contacts de 7 à 8 sec, interrompus 1 à 2 sec. La goutte liquide prend une coloration bleuâtre, mais après lavage, la surface ne contient aucune trace visible d'oxyde. Du fait de la faible valeur de la densité de courant (0.05 à 0.1 A) l'élimination des stries de préparation mécanique peut demander plusieurs minutes d'électrolyse. Dans ces conditions les contours des grains du métal recristallisé sont à peine révèlés (Fig. 18).

Pour obtenir une attaque il suffit de soumettre la surface, préalablement polie, lavée et séchée, à l'une des deux modalités suivantes:

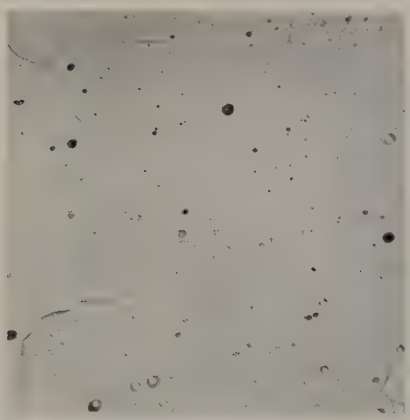

Fig. 18. Molybdène recuit 30 min à 1150°C. Polissage 2 mn avec l'électrolyte „MESUL" sous 30 V (× 400).

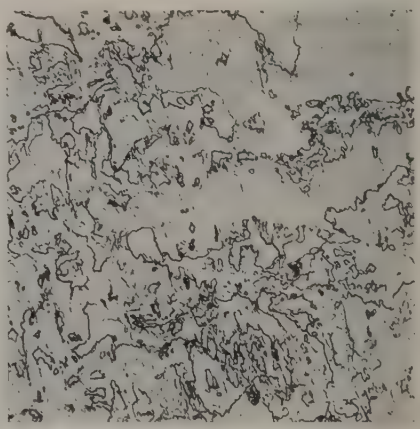

Fig. 19. Tôle de molybdène repoussée. Polissage 2 mn avec l'électrolyte „MESUL" sous 20 V suivi d'attaque pendant 35 sec (× 160).

Bibliographie p. 455

1. Application du tampon par touches à cadence assez rapide, sous une tension d'une vingtaine de Volts. La durée ne doit pas dépasser 30 à 40 sec sinon le stade initial d'attaque est suivi du polissage normal (Fig. 19).

2. La tension à vide est réglée à 3 V environ et le tampon appliqué d'une façon continue pendant un temps qui dépend de l'intensité d'attaque désirée, par exemple compris entre 60 et 90 sec. Ce moyen est susceptible de produire de petites figures de corrosion, ce qui n'est pas le cas avec la première modalité.

CONCLUSIONS

Bien que, pour ne pas allonger outre mesure l'exposé, nous ayions dû passer sous silence certains détails opératoires et nombre de résultats expérimentaux, nous espérons avoir démontré la valeur de la méthode du polissage électrolytique local appliquée aux métaux considérés ici. Il est évident que l'importance actuelle de trois d'entre eux, le béryllium, le zirconium et le zircaloy-2 justifie l'extension de cette nouvelle méthode dans les laboratoires de contrôle des matériaux nucléaires, où la simplicité de l'appareillage et la possibilité de travailler sur des objets quelconques seront particulièrement appréciées. A ce point de vue la technique de réplique au vernis apporte un complément utile, encore qu'il reste à trouver un mode d'attaque permettant l'observation des empreintes en lumière polarisée, problème déjà résolu pour l'uranium-α, autre métal anisotrope.

Grâce à la qualité des surfaces obtenues, les applications dans les domaines de la recherche n'apparaîssent pas moins intéressantes. Les exemples cités à propos des perturbations structurales induites par le travail mécanique, et des hétérogénéités révélées dans certains spécimens de zircaloy-2, sont à cet égard assez démonstratifs.

BIBLIOGRAPHIE

[1] P. A. Jacquet et A. van Effenterre, *Rev. mét.*, 54 (1957) 107; P. A. Jacquet, *Am. Soc. Testing Materials Proc.*, 57 (1957) 1290; *Rev. mét.*, 55 (1958) 531; 56 (1959) 101; *O.N.E.R.A. Note Tech.*, No. 54 (1959).

[2] P. A. Jacquet et E. Mencarelli, *Rev. mét.*, 56 (1959) 129.

[3] J. Mazia, *Steel* (1947) 84; *Monthly Rev. Am. Electroplaters' Soc.*, 34 (1947) 937.

[4] P. A. Jacquet, *Tech. Proc. Am. Electroplaters' Soc.*, (1959) 140.

[5] D. E. Bradley, *Brit. J. Appl. Phys.*, 7 (1956) 214.

[6] P. A. Jacquet et E. Mencarelli, *Compt. rend.*, 248 (1959) 2477; *Journées d'automne Soc. franç. mét.*, Paris Oct., 1959, sous presse dans *Rev. mét.*

[7] J. J. Gilman, *J. Metals*, 2, 8 (1956) 998; G. Bassi et J. P. Hugo, *J. Inst. Metals*, 87 (1959) 376.

[8] P. A. Jacquet, *Met. Rev.* 1, 2 (1956) 157.

[9] P. A. Jacquet, *Compt. rend.*, 245 (1957) 1129.

[10] P. A. Jacquet, non publié; J. Laniesse, F. Poitrat et L. Chamagne, *Colloque de Stockholm sur les matériaux de réacteurs*, Oct., 1959.

[11] J. D. Goodwin, L. S. Rubenstein, J. D. Grozier et F. L. Shubert, *U.S. Atomic Energy Comm.*, WAPD-212-UC-25-TID 4500 (1959).

[12] M. L. Picklesimer, *U.S. Atomic Energy Comm.*, ORNL 2296 (1957).

[13] P. A. Jacquet, *Recherche aéronaut.*, No. 60 (1957) 57.

[14] P. A. Jacquet, non publié.

THE NATURE AND GROWTH OF INTERACTION LAYERS FORMED DURING THE REACTION BETWEEN SOLID TITANIUM AND LIQUID ALUMINIUM

J. MACKOWIAK AND L. L. SHREIR

Battersea College of Technology, London (Great Britain)

(Received December 24th, 1959)

SUMMARY

During the interaction of solid titanium and liquid aluminium, the interaction layers have been observed to give rise to an unusual cruciform pattern. The constituents of the layers have been identified as aluminium and $TiAl_3$ by microhardness, metallographic and X-ray techniques. A thin, pervious layer of $TiAl_3$, which allows liquid aluminium to penetrate to the titanium, has been observed to be present at the titanium surface.

No diffusion of titanium into the aluminium has been detected and it would appear that $TiAl_3$ particles precipitate at the titanium surface. The position of formation of the $TiAl_3$ and the fact that its volume is greater than the volume of titanium consumed are considered to give rise to stresses in the layers resulting in rupture at the corners and the geometrical effect observed. This theory has been substantiated by quantitative studies of dimensional changes.

INTRODUCTION

The formation of a cruciform pattern by the precipitation of phases during the interaction of a solid with a liquid metal was considered, until recently, to be confined to the system solid iron- and liquid zinc[1]. However, a similar phenomenon has been observed by the authors during a study of the interaction of $Ti_{(s)}-Al_{(l)}$[2], the suffixes (s) and (l) referring to solid and liquid, respectively, (see Fig. 1).

SCHEIL[1,3,4] considered that for the Fe–Zn system the mechanism of the process was due entirely to the nature of the $FeZn_7$ layer which, in the range of approximately 470°C–520°C, formed layers completely pervious to molten Zn. Consequently, the dissolution of Fe and formation of the compound followed a linear law. BABLICK[5] suggested that the strongly orientated columnar growth of the crystals of the interaction layers was responsible for the porosity and consequent formation of the cruciform pattern.

For the $Ti_{(s)}-Al_{(l)}$ system it has been suggested[2] that the formation of a cruciform pattern could be explained by a three-stage process which involved:

(a) dissolution of Ti in Al to produce a saturated solution;

(b) precipitation of $TiAl_3$ layers, pervious to molten Al at the Ti interface;

(c) rupture of the continuous interaction layer at corners due to tensile stress.

References p. 466

It should be emphasised that there is a fundamental difference between the type of stress that occurs in an oxide film on a metal surface and the interaction layers obtained in the present work. In the case of an oxide, where the volume ratio is greater than 1, the oxide forms at the oxide–oxygen interface and the oxide is in

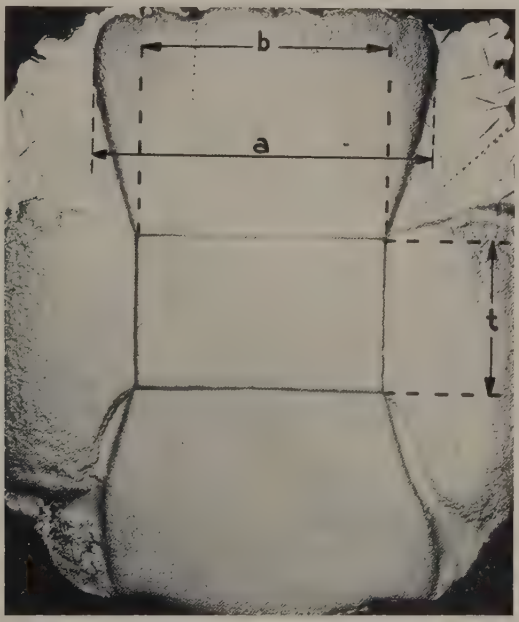

Fig. 1. Dimensions of the Ti specimen and upper part of the cruciform pattern as determined for kinetic studies. (The distortion of the other parts of the cruciform pattern is due to contact with the crucible).

compressive stress. In the present system, however, although the volume ratio of the interaction layer–metal is greater than 1, reaction and precipitation occur at the metal–interaction layer interface. This gives rise to a tensile stress in the layer as it is forced away from the metal surface.

The present work is concerned with:

(1) identification of the various phases in the interaction layer of the system $Ti_{(s)}$–$Al_{(l)}$;

(2) elucidation of the mechanism of cruciform pattern formation.

EXPERIMENTAL TECHNIQUES

Materials

Analyses of the superpurity Al, Ti 130 and Ti 150A used in the present work are given in Table I.

References p. 466

TABLE I

Material	*Element*	*Wt-%*
Ti 130	H_2	0.0037
	C	0.05
	Fe	0.035
	Cu	0.01
	Sn, Mn, Al	(not detected)
	Mg	0.05–0.1
	Si	0.01–0.05
	Ti	99.75
Al (superpurity)	Al	99.99
	Si	0.001–0.002
	Fe	0.005–0.0015
	Cu	0.001–0.0015
Ti 150A	(nominal composition)	
	Ti	96
	Cr	2.68
	Fe	1.32
	O	0–0.2
	N	0.02

Preparation of specimens

The Ti specimens used were in the form of cylinders, 9 mm diam. × 4–5 mm long. They were abraded down to 0000 carborundum using water as a coolant and finally polished on a selvyt-covered wheel with a proprietary metal polish. The specimens were then well washed with cold tap-water and soap, rinsed and dried, using acetone and a stream of cold air, and stored in a dessicator over calcium chloride. Prior to dissolution-annealing, the dimensions were measured accurately with a micrometer.

The Al used was in the form of a cylinder having a hole of diameter slightly smaller than the Ti specimen drilled in one end. By applying pressure, the Ti specimen could be forced into the hole so that it was in intimate contact with the Al. The composite specimen, which fitted into a Morgan XN1O alumina crucible, was then dissolution-annealed, cooled in vacuo (less than 10^{-3} mm Hg) and finally cut longitudinally by means of a hacksaw. Specimens prepared in this way were mounted in bakelite and the cut face polished for metallographic examination. No etching was necessary to reveal the contour of the interaction layer.

Examination of the specimens

The specimens obtained during the study of the kinetics of cruciform pattern formation were examined using metallographic, microhardness, spectrographic and X-ray techniques.

Metallographic studies

An aqueous solution containing 1.5% of hydrofluoric acid and 3% of nitric acid was found satisfactory for etching the specimens to reveal the structure and was used throughout this work.

Microhardness studies

A standard bench-type microhardness tester was used, the load in general being 100 g.

References p. 466

Specimens were carefully repolished before hardness testing and any surface hardening caused by the repolishing was removed by etching.

X-ray studies

(a) Powder technique. Samples obtained by carefully filing the area under investigation were found to be suitable for X-ray powder studies without further annealing.

The patterns obtained from the unknown phases were then compared with standards

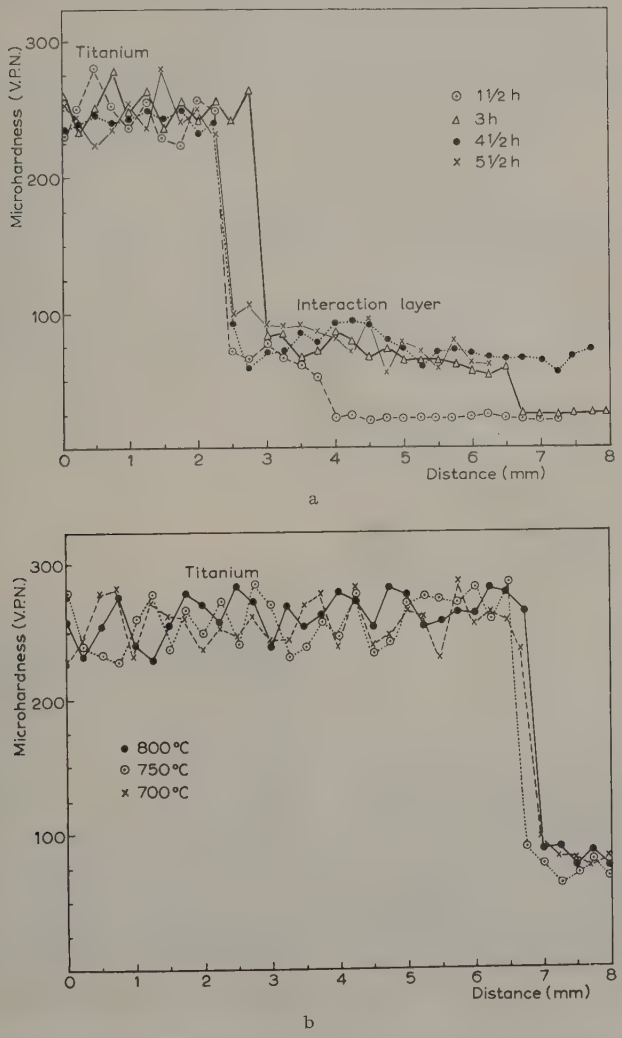

Fig. 2. Variation of microhardness with distance from a point within the Ti specimen: (a) constant temperature (800°C), variable time; (b) variable temperature, constant time ($4\frac{1}{2}$ h).

References p. 466

obtained using Al (superpurity), $TiAl_3$, and Ti 130. As the lines on the patterns obtained from the unknown phases coincided completely with the standards no indexing of the diffraction patterns was necessary.

(b) Back-reflection technique. The diffraction patterns in the X-ray back-reflection method were interpreted by matching with patterns obtained from standard samples of superpurity Al, $TiAl_3$ and Ti 130 obtained under the same conditions. The relative grain sizes of any of the phases were estimated from the number of spots in the appropriate rings in the diffraction patterns, and the orientation of the phase was deduced from the distribution and shape of the spots.

For the microbeam X-ray back reflection studies, an Ehrenberg and Speer fine-focus X-ray tube was used, given a focal spot of about 40 μ. The beam was aligned with the small area to be irradiated using the method described by LEWIS[6].

PHASES PRODUCED DURING DISSOLUTION ANNEALING

Titanium

Metallographic examination of the Ti specimens after dissolution-annealing revealed that the surface of the Ti had dissolved uniformly, *i.e.* there was no intergranular attack.

The absence of Al in the Ti lattice was confirmed by a series of microhardness measurements using specimens prepared isothermally at 800°C for different periods of time (Fig. 2a) and at different temperatures for a constant time of $4\frac{1}{2}$ h (Fig. 2b).

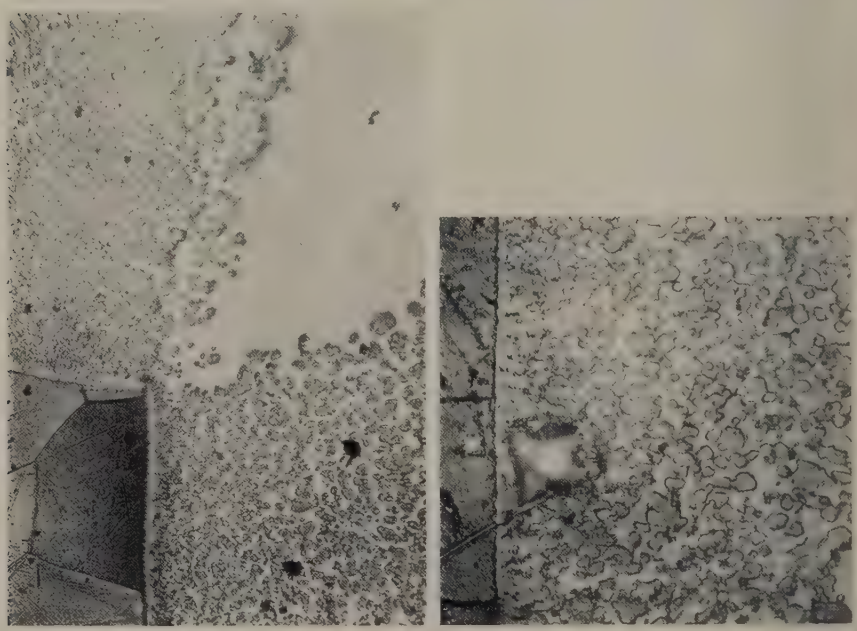

a b

Fig. 3. Microstructure of the interface and the interaction layer of a specimen prepared at 850°C, $5\frac{1}{2}$ h: (a) magnification × 120 (Ti – lower left hand corner, Al white); (b) magnification × 500.

References p. 466

A careful microhardness examination of the Ti adjacent to the Ti–Al interface revealed no increase in the hardness of Ti, indicating that there was no detectable diffusion of Al into the Ti. This was confirmed by spectrographic analysis of samples obtained near the interface.

From the above results, it is evident that there is (a) no significant diffusion of Al into Ti, (b) no preferential dissolution of certain phases from the Ti surface, and (c) no intergranular penetration by the Al.

NATURE OF INTERACTION LAYERS

An examination of the microstructure of the surface of the cruciform pattern revealed that, in addition to the layer constituting the cruciform pattern, a very thin layer ($\approx$ 10 μ) of higher hardness was present adjacent to the Ti surface. Typical micrographs of this thin uniform layer at different magnifications are shown in Figs. 3a and 3b and it is apparent that the thin layer completely surrounds the Ti specimen. It would appear that this layer is not continuous but consists of longitudinal crystals orientated in a direction that is almost perpendicular to the Ti surface. It is possible that, in view of the structure, this layer is permeated by capillaries which terminate at the Ti surface. Although it is considered that this layer is present during dissolution-annealing the possibility that the capillaries and the thin interaction layer may form during cooling should not be precluded. An X-ray microbeam examination showed that the thin interaction layer surrounding the Ti contained two phases:

(a) large crystals (10 to 20 μ) which were identified as $TiAl_3$;

(b) small crystals ($<$ 1 μ) which were identified as Al.

Examination of specimens prepared at temperatures ranging from 800°–900°C revealed that the $TiAl_3$ crystals were of uniform size (Table II) and randomly orientated, whereas the Al crystals had a preferred orientation.

TABLE II

NUMBER OF SPOTS ON MICROBEAM DIFFRACTION PHOTOGRAPHS

Temp. °C	*Number of spots on microbeam diffraction photographs*			
	Ring I	*Ring II*	*Ring III*	*Total*
800	14	11	8	33
850	12	12	11	35
900	14	12	6	32

The measured hardness of the thin interfacial layers was around 550, and as the recorded hardness of $TiAl_3$ is also about 550 it is logical to assume that if any Al is present in the layers the quantity is not sufficient to affect its hardness, and that the Al is probably confined to the capillaries only.

The effect of time and temperature on the thickness of the interfacial layer is shown in Tables IIIA and IIIB. These results must be regarded, however, as only approximations owing to the ill-defined boundary between the thin layer and the interaction layer of the cruciform pattern (Fig. 3b).

References p. 466

TABLE IIIA

THICKNESS OF LAYER AT 850°C (CONSTANT TEMPERATURE)

Time of dissolution annealing (h)	*Thickness (mm)*
1·5	0.014–0.016
3.0	0.014–0.016
4·5	0.014–0.016
5·5	0.014–0.016

TABLE IIIB

THICKNESS OF LAYER AT CONSTANT TIME ($4\frac{1}{2}$ h)

Temperature °C	*Thickness (mm)*
850	0.014–0.016
800	0.010–0.012
750	0.008–0.010
725	0.006–0.007
700	0.006

It would appear that the thickness of the continuous diffusion layer around the Ti surface is a function of temperature but is independent of time. It was observed that, at all temperatures investigated, the number of microcapillaries per unit length of interface was constant, *i.e.* 250–300 per mm.

LAYER CONSTITUTING CRUCIFORM PATTERN

From a metallographic examination, it was evident that this layer consisted of a crystalline precipitate embedded in a matrix and that the particle size of the precipitate increased considerably with the distance from the Ti interface. From a consideration of the Ti–Al phase diagram it would appear that the only two possible compounds which could exist under these conditions are TiAl and $TiAl_3$ in a solid solution of Ti in Al.

The hardness of the particles, obtained by several independent measurements was 540–560, which is in good agreement with the recorded value for $TiAl_3$[7], while that of the matrix was 20–23. It thus appears that the cruciform pattern consists of particles of $TiAl_3$ in an Al matrix. This conclusion was confirmed by X-ray powder photographs of specimens prepared at different temperatures and times and, in all cases, it was found that only lines corresponding with $TiAl_3$ and pure Al were present. As the solubility of Ti in Al at room temperature is practically negligible any solid solution existing at the annealing temperature thus probably decomposes on cooling into Al and $TiAl_3$.

X-ray back-reflection photographs of the interaction layers produced during the dissolution of Ti 130 or Ti 150A in molten Al showed that the cruciform pattern consisted of $TiAl_3$ particles randomly orientated in an Al matrix and that the particle size of the $TiAl_3$ increased considerably with increasing distance from the Ti–Al interface. It seems, therefore, that initially very fine particles of $TiAl_3$ are formed continuously at or near the interface. These are forced away from the interface by precipitation of further particles and continue to grow during the heating operation.

References p. 466

From the diffraction patterns it was observed that the grains of Al near the Ti surface were strongly orientated and that their orientation became more random with increasing distance from the Ti surface. Their size, however, decreased with the increasing distance from the interface.

It can be concluded from the examination of the dissolution-annealed specimens that there is no detectable diffusion of Al into Ti and no preferential dissolution or pitting of the surface of the Ti. A thin interaction layer develops around the Ti surface whose thickness appears to be independent of time but is a function of temperature. This layer consists of columnar $TiAl_3$ particles of random orientation; the size of these particles in specimens prepared at different temperatures is of the same order of magnitude, and increases rapidly with their distance from the Ti–Al interface. There are capillaries in the layer which appear to contain a second phase and this is probably Al. The cruciform pattern consists of $TiAl_3$ particles in a matrix of Al. No evidence could be obtained of the formation of phases other than $TiAl_3$, either for Ti 130 or 150A.

DIMENSIONAL CHANGES DURING CRUCIFORM PATTERN FORMATION

It was thought that owing to the unusual symmetry of the cruciform pattern measurements of dimensional changes might provide a simple method of verifying the mechanism previously proposed[2]. According to the latter, the difference in width (a—b) (Fig. 1) should be identical with the decrease in the width ($\triangle$t) of the Ti specimen (which dissolved uniformly on all faces) provided there is no distortion of the pattern by mechanical forces, by redistribution of phases within the layer with time, by crystalline growth or by considerable dissolution of $TiAl_3$ in molten Al.

Measurements of dimensional changes are reported in Table IV.

The results (Table IV) show that at the higher temperatures, providing the anneal-

TABLE IV

DIMENSIONAL CHANGES DURING THE FORMATION OF A CRUCIFORM PATTERN

Temp. (°C)	*Time of anneal* (h)	$(a-b)$ (mm)	*Decrease in thickness* ($\triangle t$) (mm)	$(a-b)-\triangle t$ (mm)
Ti 150A				
800	1.0	0.62	0.58	0.04
	2.0	1.62	1.60	0.02
	3.0	2.73	2.61	0.12
Ti 130				
850	3.0	0.97	0.96	0.01
	4.5	1.76	1.69	0.07
	5.5	2.20	2.13	0.07
800	1.5	0.33	0.28	0.05
	3.0	0.72	0.64	0.08
	4.0	1.09	0.97	0.12
	5.5	1.53	1.43	0.10
750	4.0	0.80	0.65	0.15
	5.0	1.11	0.81	0.30
	7.2	1.70	1.28	0.42
700	4.0	0.51	0.31	0.20
	7.0	0.92	0.62	0.30

References p. 466

ing time is not prolonged, $(a - b) - \triangle t \approx 0$. The mechanism proposed previously is thus confirmed by these measurements.

DISCUSSION OF RESULTS AND MECHANISM

From the results obtained in the present work, it is apparent that an essential factor for cruciform pattern formation is that the precipitated layers formed during dissolution should be porous. Similar considerations apply to the $Fe_{(s)}$–$Zn_{(l)}$ system. This porosity permits the molten metal to penetrate to the reaction interface resulting in a rate of dissolution that is constant. It is of interest to note that in both systems the solubility of the solid metal and their compounds in the liquid metal is very small at the experimental temperatures[8].

ELDRED[10] considers that atoms at edges or corners are likely to pass into solution more readily than those from the centre of a lattice and concludes that rounding of corners is to be expected in diffusion processes. SCHEIL AND WURST[4] postulate a non-diffusion process of dissolution to explain the fact that no rounding of corners occurs during the dissolution of Fe in molten Zn.

From the above considerations, it is reasonable to assume that in the Ti–Al system, as the corners and the original shape of the specimens are preserved, there is little likelihood of diffusion of Ti into the molten Al. It is, therefore, more probable that a surface reaction takes place.

The fact that no Al was detected in the Ti may be explained by assuming that the rate of precipitation of $TiAl_3$ at the interface is much faster than the rate of diffusion of Al into Ti. It is of interest to note that only $TiAl_3$ was found to be present, although several other phases are indicated by the equilibrium diagram. It is possible, however, that during the surface reaction other phases may be present but decompose on cooling into Al and $TiAl_3$. Alternatively, the amounts present in the solidified interaction layer may be so small that they could not be detected by the techniques used in the present work.

GRAY[9] considers that thermodynamical reasoning does not provide a reliable criterion for predicting the possible reaction products when the system is not at equilibrium. In the present work, the continuous precipitation of $TiAl_3$ may thus explain the absence of phases which, from the equilibirum phase diagram, would be expected to be present. In addition, from kinetic considerations, it may be possible that a low energy of activation for the formation of $TiAl_3$ compared with the other possible compounds is responsible for the preferential formation of this phase.

The X-ray microbeam studies, which show that the crystals composing the interaction layer surrounding Ti are not preferentially orientated, are of particular interest as in the $Fe_{(s)}$–$Zn_{(l)}$ system it was considered[5] that the strongly orientated columnar growth of this layer was responsible for the porous nature of the $FeZn_7$ layer.

MECHANISM OF THE CRUCIFORM PATTERN FORMATION

The previous predictions[2] regarding the probable mechanism of cruciform pattern formation have been confirmed for Ti 130 and Ti 150A at temperatures of 850° and 800°C. However, at lower temperatures it is apparent from Table IV that the dimension $(a - b)$ of the pattern is greater than would be expected from $\triangle t$, the

References p. 466

discrepancy being most prominent at the lowest temperature studied (700°C). The mechanism of the cruciform pattern formation thus appears to be far more complex than considered previously. In particular, the rate of growth of the $TiAl_3$ particles in the layers must be taken into account in explaining the unexpectedly high value of "a" (see Fig. 1). It would appear that the slower the rate of growth of the layers, the larger is the deviation of "a" from its predicted value. This may be due to the growth of the $TiAl_3$ particles in the interaction layer resulting in an increased value of "a".

In the light of the evidence obtained it appears unlikely, therefore, that the first step of the cruciform pattern formation is the formation of a saturated solution of Ti in molten Al. It is concluded from the present work that the formation of the cruciform pattern occurs by a four-stage mechanism (Fig. 4):

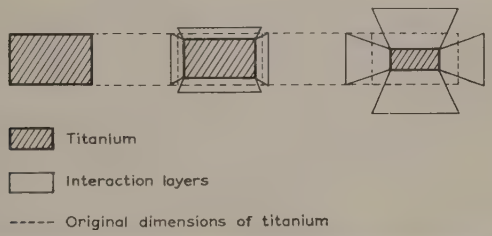

Fig. 4. Diagrammatic representation of the various stages during cruciform pattern formation.

(1) A reaction between $Ti_{(s)}$ and $Al_{(l)}$ on the surface of the Ti results in a thin interaction layer which is pervious to Al.

(2) The compound already precipitated is forced away from the Ti surface. This is attributed to the development of tensile stress in the interaction layer parallel to the Ti surface, arising through the continuous precipitation of $TiAl_3$ at the interface and the fact that the volume of the precipitate is much greater than that of the dissolved Ti.

(3) Rupture of the interaction layer at the corners resulting from the tensile stress in the coninuous layer exceeding the attractive force between particles of $TiAl_3$.

(4) Concurrent precipitation and breakdown leading to the production of a cruciform pattern.

This is believed to offer a reasonable explanation of the mechanism responsible for the cruciform patterns observed in this work. An exact prediction of the dimensions of the cruciform patterns formed at lower temperatures is not possible as other factors then contribute to dimensional changes in the growing layers.

ACKNOWLEDGEMENTS

Grateful acknowledgement is made to Dr. D. LEWIS for carrying out the microbeam X-ray studies, to Diffusion Alloys, Ltd. for financial support and to Dr. O. KUBASCHEWSKI and Mr. R. SAMUEL for helpful discussions.

References p. 466

REFERENCES

1 E. SCHEIL, *Z. Metallk.*, 27 (1935) 76.
2 J. MACKOWIAK AND L. L. SHREIR, *Acta Met.*, 4 (1956) 556.
3 W. PUNCEL, E. SCHEIL AND R. STENKOFF, *Arch. Eisenhüttenw.*, 9 (1935) 301.
4 E. SCHEIL AND H. WURST, *Z. Metallk.*, 29 (1937) 224.
5 H. BABLICK, *Galvanizing (Hot Dip)*, 3rd Ed., E. & P. N. Spoon Ltd., London, 1950.
6 D. LEWIS, *J. Sci. Instr.*, 32 (1955) 467.
7 H. R. OGDEN, D. J. MAYKUTH, W. L. FINLAY AND R. I. JAFFEE, *J. Metals*, 3 (1951) 1150.
8 J. MACKOWIAK, Unpublished work (Ph.D. thesis).
9 T. J. GRAY, W. P. DETWILER *et al.*, *The Defect Solid State*, Interscience Publishers Inc., New York and London, 1956.
10 V. W. ELDRED, Ph. D. THESIS, 1953, Cambridge University.

AN INVESTIGATION OF THE NEPTUNIUM–URANIUM EQUILIBRIUM DIAGRAM

P. G. MARDON AND J. H. PEARCE

Atomic Energy Research Establishment, Harwell, Berks. (Great Britain)

(Received December 5th, 1959)

SUMMARY

The general form of the neptunium–uranium diagram has been determined by thermal analysis, dilatometry and X-ray techniques, using a very limited amount of neptunium. The results show that there is high solubility of uranium in the α and β phases of neptunium and of neptunium in the α and β phases of uranium; the room temperature solubility of neptunium in α-uranium has the unusually high value of 43 wt-%. Some uncertainty exists as to whether or not there is complete solid solubility between γ-neptunium and γ-uranium but any miscibility gap is definitely very restricted.

There is one intermediate phase in the system, stable up to temperatures around 650°C and existing between 75 and 48 wt-% neptunium at room temperature. Its crystal structure is simple cubic (a = 10.6 Å) and it is isomorphous with the ζ phase in the plutonium–uranium system.

1. INTRODUCTION

During 1957 approximately 18 g of neptunium metal (^{237}Np) were made available for chemical and metallurgical research at A.E.R.E., Harwell. This material had been recovered from the residues of the plutonium extraction plant at Windscale and its extraction has been described elsewhere[1].

The isotope ^{237}Np is an α-emitter with a half life of $2.5 \cdot 10^6$ years. It is a highly toxic material comparable to ^{239}Pu and for this reason, the work on the metal is being carried out in glove boxed equipment. The initial metallurgical programme at Harwell consisted of rechecking the published U.S. data on phase transitions and crystal structures[2,3], followed by the determination of certain physical properties[4,5,6]. A part of the material was then allocated for a study of the alloying behaviour of the metal and it was decided that the material available could be most profitably employed in determining the effect of alloying with other members of the actinide series. The first of these to be tried was uranium and the results are given in the present paper; a start has also been made on extending this work to alloys with plutonium.

The amount of metal to be used in any one system has been limited to 2–3 g. This has severely restricted the choice of available techniques and the proposed diagram may not be correct in detail. In general the techniques adapted were such that there was only a limited loss on any specimen after testing, and in fact at the end of the work approximately 50% of the neptunium was in a recoverable form.

References p. 475

2. EXPERIMENTAL METHODS

(*a*) *Preparation of alloys*

Initially two alloys each weighing about 1 g, were prepared by argon-arc melting of the parent metals. The first alloy contained 1 wt-% uranium and the second one 50 wt-% uranium. After carrying out the required experiments on each of these alloys, they were remelted to give alloys slightly richer in uranium. By a repetition of this method it was possible to cover the whole range of composition from the two original alloys. In general the interval between successive alloys was of the order of 2–3% uranium. It would have been possible to cover the whole system from a single neptunium-rich alloy, but it was felt that the increased expenditure of neptunium in having two alloys available at one time was justified by the increased rate of working and by providing a check on the initial results in the case of the more uranium-rich alloys.

The uranium additions required to convert one alloy into the next were only in the range 25–50 mg for the neptunium-rich part of the system where melting losses were of the order of 2 mg, whilst for alloys in the middle of the diagram the uranium additions were 50–75 mg, the losses being 15–30 mg; thus if all the loss was uranium a serious error in composition would occur after 5 or 6 remelts. The good agreement for the 50/50 region between the original 50/50 alloy and the many times remelted original neptunium-rich alloy indicates that this was not so and that the loss must therefore have been spread over the whole alloy. Material could not be spared for analyses of the alloys until the work was completed, at which time both alloys were very uranium-rich and an analytical check would have had little bearing on the difference between intended and actual compositions at an earlier stage of the work. Spectroscopic analysis was however carried out to see whether pick up of impurities had occurred during the arc melting and thermal analysis processes respectively. The results of this are given in section 3(c). The chief impurities in the neptunium were 0.34 wt-% calcium and 0.22 wt-% uranium whilst the uranium was standard Springfields uranium which had been arc melted prior to use; the major impurities were carbon 250 ppm, aluminium 90 ppm and iron 50 ppm.

(*b*) *Thermal analysis and dilatometry*

An apparatus for doing combined thermal analysis and dilatometry with automatic recording was developed for work with plutonium alloy samples on a scale of 5–10 g and this has been described elsewhere[7]. With the small 1 g samples of the neptunium alloys, the apparatus proved to be satisfactory although the dilatometer had to be operated at its maximum sensitivity (5000 × amplification on the recorder). For temperatures up to 950°C, chromel–alumel couples were used and checked at frequent intervals on the melting point of aluminium and less commonly on that of silver. For work above 950°C, platinum–platinum-13% rhodium couples were used and standardised at the melting point of gold.

It was interesting to observe that the latent heat of the solid state transitions was generally greater than that of melting as shown by the larger "kicks" for the former on the differential thermal analysis. Except at the uranium-rich end, the liquidus was only determined at infrequent intervals to reduce to the minimum any reaction between the molten alloy and the alumina crucible and thermocouple sheath.

For solid state changes, all values were taken on heating runs due to the uncer-

References p. 475

tainty produced by hysteresis on cooling. The rate of heating was kept to 2°C per minute or less to reduce any error in the values obtained and the width of the two phase regions was assessed from the start of the "kicks" and the point at which the deflection started to decrease; both of these values probably err on the low side but by standardizing the couples under similar conditions on aluminium, the corrected value was almost certainly correct to better than 5°C.

(c) X-ray techniques

Two powder cameras were employed in the investigation, a Guinier focussing camera for room temperature work[8] and a high temperature camera. In general the changes of lattice parameter across the single phase fields of the system were too small to be of use in fixing the boundaries of these regions so that the disappearing phase technique had to be used. The low background and generally high quality of the films taken in the Guinier camera allowed the room temperature boundaries of the various phases to be determined with moderate accuracy although the method was complicated by the slow rate of precipitation of the intermediate δ phase from α-neptunium at temperatures below 150°C and at the uranium-rich end of the diagram by unfortunate coincidences between certain strong lines of α-uranium and of the δ phase.

The high temperature camera was based on the well-known Unicam type but with modifications designed to make it safer for handling α-active specimens; it also included certain other features such as re-aligning of the specimen when the camera was under vacuum. The quality of the films obtained was poor by normal standards due to the readiness with which neptunium and its alloys oxidize, the heavy secondary emission from the specimen and its natural β-γ emission. From the standpoint of oxidation the metal behaved in a manner comparable to plutonium and at temperatures near the melting point it showed an unfortunate tendency to react with the silica capillaries.

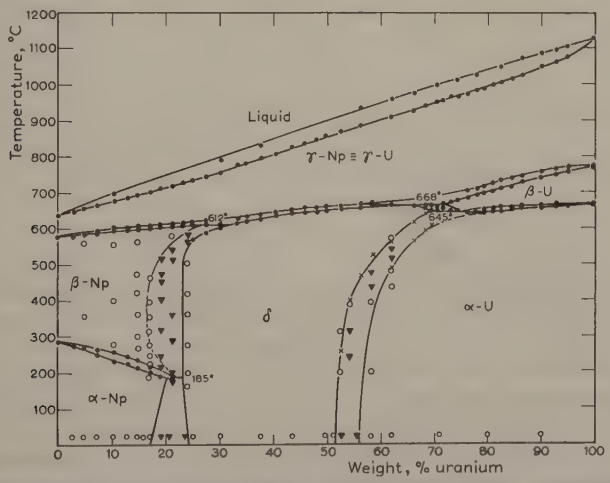

Fig. 1. The neptunium–uranium system: • thermal analysis transitions; × dilatometric transitions; ▼ 2 phase alloys (X-ray data); ○ single phase alloys (X-ray data).

References p. 475

(d) Pyknometry

The conventional displacement method was used, ethylene dibromide being the liquid employed. Owing to the small size of the samples and the difficulty of completely removing the oxide skin without serious loss of the actual alloy, it was not possible to determine the density with certainty to better than 0.05–0.1 g/cm³. The method was used only to give a general survey of the density variation with composition at room temperature.

3. RESULTS

The proposed equilibrium diagram for the system is given in Fig. 1. It has been drawn principally on the basis of the thermal analysis results, the other experimental data having been used as confirmatory evidence and for determining the boundaries of the single phase fields. Fig. 2 shows the results of density determinations across the whole of the system. In general, the accuracy of the compositions of phase boundaries is approximately ±1%.

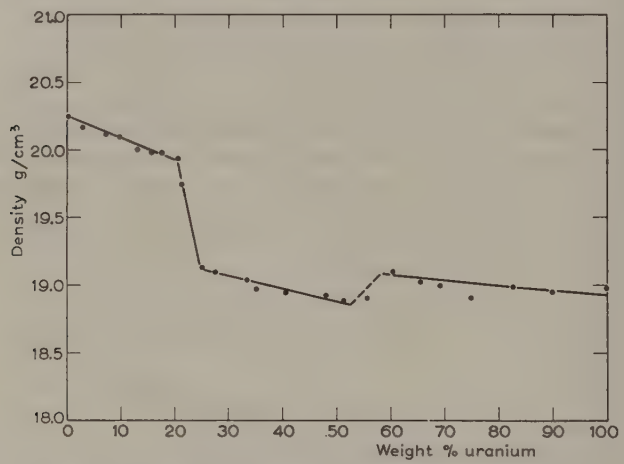

Fig. 2. Density–composition curve (room temperature).

(a) The α- and β-neptunium fields

There is considerable solubility of uranium in both α- and β-neptunium accompanied by depression of the $\alpha \rightarrow \beta$ transition temperature. The disappearing phase technique suggests that the limit of the α-field at room temperature is about 17% uranium whilst lattice parameter measurements suggest a value of 15 ± 2%; the difficulty of using the latter method is shown in Fig. 3, the scatter of the results being sufficient to mask the boundary point. An interesting feature is that the density measurements suggest a value of 20% uranium for the boundary, presumably due to uranium being retained in super-saturated solution at room temperature in the relatively massive specimen as compared with the filings employed in the X-ray work.

References p. 475

The thermal analysis results suggest that the solubility increases to 20% uranium at the β-eutectoid temperature (185°C) as expected from the density determinations.

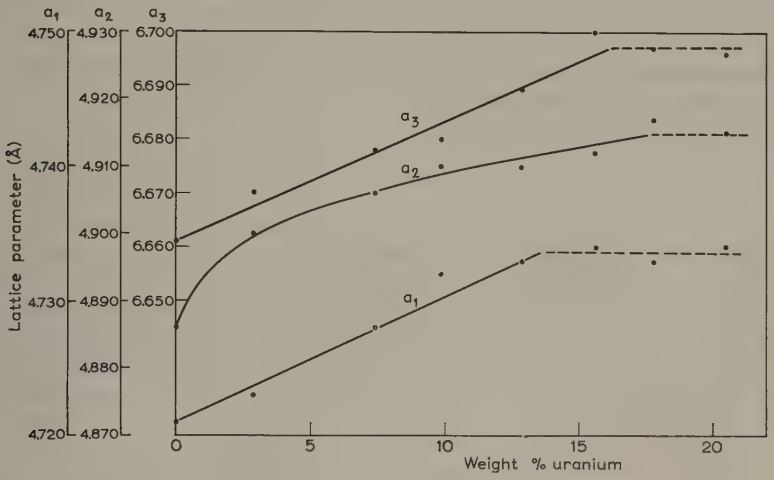

Fig. 3. Lattice parameter–composition curves, α-neptunium field.

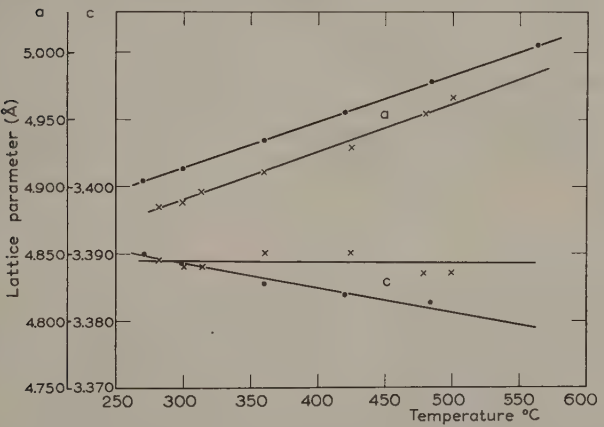

Fig. 4. Lattice parameter–temperature curves for β-neptunium: • neptunium 14.9 wt-% uranium alloy; × pure neptunium (ZACHARIASEN's values).

The solubility limits of the β-neptunium field have been determined by means of high temperature X-ray photographs. There is very little change in cell side or thermal expansion coefficients across the field, as shown in Fig. 4. However, the results on a 17% uranium alloy were very informative: filings were annealed at 500°C, cooled to 210°C and a series of photographs taken with rising temperatures; below 280°C and above 360°C the patterns were sharp and of single phase β but between these

References p. 475

two temperatures the patterns were heavily strained. No line of any phase other than β-neptunium could be identified but the straining was taken as evidence of precipitation of another phase occurring, thus implying that the solubility of uranium in the β-phase first decreases and then increases as the temperature is raised. At the high temperature end of the field, the boundary curves over sufficiently to be detectable by thermal analysis and the latter technique indicated a maximum solubility of about 26% uranium at the β-peritectoid (613°C) where the phase decomposes into γ-neptunium and the intermediate δ phase.

(b) The δ phase

This is the only intermediate phase present in the system and extends over a large part of the middle of the diagram; the limits of its field at room temperature are 24% and 52% uranium. On the neptunium-rich side of the field, the boundary only varies slightly with temperature up to 550°C, but is then displaced rapidly towards the uranium-rich end of the system. The phase decomposes by a peritectoid reaction into γ-neptunium and β-uranium at 668 $\pm$ 3°C. The uranium-rich boundary curves off steadily to higher uranium contents with rising temperature, reaching a maximum of 69% uranium at 645°C.

Structurally the phase is isomorphous with ζ plutonium–uranium[9], being simple cubic at room temperature. The behaviour at high temperatures is similar to that of ζ plutonium–uranium, line splitting occurring; however attempts to index these lines unambiguously on a large tetragonal cell with c/a close to unity have proved difficult but it seems probable that c/a increases from unity at room temperature to about 1.02 at 500°C. There is a slight variation of lattice parameter with composition across the field, the room temperature value increasing from 10.55 Å at 25% uranium to 10.63 Å at 50% uranium; this variation is paralleled by the macroscopic density changes over this composition range as shown in Fig. 2. The actual value of the macroscopic density for any one alloy is generally 0.2–0.3 g/cm^3 lower than the theoretical X-ray density and this phenomenon also occurs for the other room temperature phase fields.

(c) The γ-neptunium–γ-uranium field

The present authors originally reported[10] that complete solid solubility occurred between γ-neptunium and γ-uranium. Subsequent thermal analysis results from specimens derived from the 50/50 alloy seemed to indicate a small miscibility gap at the uranium-rich end as shown by a horizontal portion of the solidus. This result was very surprising in view of the strong possibility that γ-neptunium and γ-uranium are isostructural[3] with a size factor even more favourable than that associated with ε-plutonium and γ-uranium, a system in which complete solid solubility is known to occur[11,12]. Attempts to observe the structures present by means of the high temperature X-ray camera were unsuccessful due to the readiness with which the alloys oxidise at temperatures above 600°C and no signs of the boundaries of the two phase γ-neptunium + γ-uranium field were observable by dilatometry. The thermal analysis results were then carefully rechecked using the original neptunium-rich alloy: no signs of a horizontal were observed in the solidus, which instead rose smoothly to the melting point of uranium. The existence of a eutectoid reaction by which γ-uranium

References p. 475

decomposed into γ-neptunium and β-uranium, as postulated for the case of the miscibility gap, had always been very uncertain in thermal analysis, so that no definite conclusions about the existence of the gap could be drawn from the presence or absence of this reaction. Small samples of both the alloys were sent for spectroscopic analysis to determine whether or not the miscibility gap could have been produced by contamination of the first of the two alloys. Both were found to contain small amounts of silica and iron (of the order of 500 p.p.m.) whilst the suspect alloy also contained 2000 p.p.m. of molybdenum. Two other possible contaminants, tantalum and tungsten, were not detectable but owing to the low sensitivity for tantalum, up to 0.5 wt-% of the element could be present. Since molybdenum is extensively soluble in γ-uranium, it seems difficult to attribute the miscibility gap to the small amount of this element present in the one case.

With the exception of the solidus and the possible γ-uranium eutectoid reaction, all the other arrests were essentially the same for the two alloys, the maximum differences in temperature being about 5°C and these could well be due to the uncertainties in composition of the two alloys. Without using fresh neptunium it is not possible to prove beyond doubt that the complete solid solubility result is correct, but since this seems to be the more probable case, the present diagram has been drawn up on this basis.

(d) The α- and β-uranium fields

There is high solubility of neptunium in both α-uranium and β-uranium, accompanied by a slight depression of the $\alpha \rightarrow \beta$ transition temperature. Because of this it is difficult to detect the uranium-rich limit of the β-eutectoid reaction which occurs at 645 ± 5°C. The maximum solubility in the β phase is 26% neptunium, whereas for the α phase the value increases steadily as the temperature falls from the β-eutectoid temperature, the solubility reaching a maximum of 43% neptunium at room temperature. The limits of the two phase α-uranium $+ \delta$ phase field were determined by dilatometric and X-ray examinations and the results of the two methods were in reasonable agreement.

The variation in lattice parameters across the α-uranium field was determined but the results showed considerable scatter. It was however clear that the addition of neptunium caused a slight contraction of the orthorhombic unit cell along all three axes, with a resultant increase in density. The maximum density would thus occur at the limit of the α field and the calculated value at this point is of the order of 19.4 g/cm^3. The macroscopic density results for the α-uranium field were not very good, probably due to entrapment of oxide in the frequently remelted alloys, but nevertheless they do show some increase in density as the neptunium content is raised.

The effect of temperature on the lattice parameters of a 40% neptunium alloy closely parallels its effect on the pure α-uranium parameters, a and c increasing markedly whilst a slight contraction occurs in the value of b.

4. DISCUSSION

Several interesting features are exhibited by this system and a comparison may be made with other uranium alloy systems in general and the plutonium-uranium system in particular.

References p. 475

The solubility of other elements in α-uranium is generally very low, rarely exceeding 2 at-%[13]. Plutonium was the first element found to have appreciable solubility in α-uranium (12% at room temperature) and the very high solubility of 43% for neptunium suggests that the actinide elements may form an exception to the general rule. This would not be altogether surprising in view of the highly directionalised bonding of α-uranium, which suggests that only elements capable of forming such bonds would be soluble in this phase. This would also be expected to hold for solutions of actinide elements in the other low temperature complex structures formed by these elements *e.g.* α-neptunium and α-plutonium. The present results show that this is true for the case of uranium dissolving in neptunium but it is certainly not always true, as evidenced by the low solubility (probably about 1%) of uranium in α-plutonium. It is possible that this is associated with a change in the nature of the bonding as one progresses along the actinide series, the outermost electrons having a more pronounced *f* character and correspondingly less *d* character in the higher members as compared with uranium. Thus plutonium in its alloying behaviour is more variable than uranium and this adaptability of the plutonium atom may account for the much higher solubility of plutonium in α-uranium as compared with that of uranium in α-plutonium. If sufficient quantities of americium and curium eventually become available, it would be very interesting to extend these studies of mutual solubilities.

The δ phase is isostructural with ζ plutonium–uranium, the structure of which was unique when first discovered[9] and even now, comparatively little is known about it; indeed Russian investigators[14] do not agree with the structure proposed by COFFINBERRY, but the work of the present authors agrees with the U.S. results. The lattice parameters are almost identical in the two alloy systems mentioned and the splitting of lines on increase of temperature is observed in both cases. Work on the neptunium–plutonium system[15] has not yet shown the existence of such a phase at room temperature. However two compounds may exist at the plutonium-rich end at higher temperatures[15,16] and there is an unsurveyed region of the diagram between 90 and 55% of neptunium in which the results from the alloys on either side suggest that a compound probably occurs; there is thus an appreciable possibility that one of these compounds has the ζ plutonium–uranium structure. If this proves to be the case, it will indicate that this structure is of major importance in alloys between actinide elements and in spite of the poor quality of the X-ray photographs so far obtained for this phase, it might be worthwhile attempting a full structural analysis.

No intermetallic phase exists in the neptunium–uranium system analogous to the higher temperature η plutonium–uranium phase. This phase gives extremely poor X-ray patterns[9,15] and no definite structure has been assigned to it; it will therefore be difficult to detect phases isostructural with it in other alloy systems.

The present work has indirectly thrown some light on the problem of the structure of γ-neptunium. ZACHARIASEN[3] has pointed out that if it is body-centred cubic, as seems most likely by comparison with the highest temperature allotropes of its neighbours uranium and plutonium, then its probable lattice parameter is such that every line except one of the pattern is obscured by those of the oxide, NpO. However if ZACHARIASEN's proposed structure is correct, one would expect complete miscibility to occur with both γ-uranium and ε-plutonium. The present results suggest that this is so for γ-uranium and if this also proves to be true for ε-plutonium the last doubts about the structure of γ-neptunium will have been removed.

References p. 475

ACKNOWLEDGEMENTS

The authors wish to thank Mr. F. T. BIRKS for carrying out the spectroscopic analyses, Mr. J. A. C. MARPLES for the Guinier camera photographs and Dr. M. B. WALDRON for his interest in the work.

REFERENCES

1 J. S. NAIRN, D. A. COLLINS, H. A. C. MCKAY AND A. G. MADDOCK, *Proc. Intern. Conf. Peaceful Uses Atomic Energy, Geneva*, 17 (1958) 216.
2 E. F. WESTRUM AND LE ROY EYRING, *J. Am. Chem. Soc.*, 73 (1951) 3399.
3 W. H. ZACHARIASEN, *Acta Cryst.*, 5 (1952) 660, 664.
4 J. P. EVANS AND P. G. MARDON. *Phys. and Chem. Solids*, 10 (1959) 311.
5 J. A. LEE, P. G. MARDON, J. H. PEARCE AND R. O. A. HALL, *Phys. and Chem. Solids*, 11 (1959) 177.
6 J. A. LEE, J. P. EVANS, R. O. A. HALL AND E. KING, *Phys. and Chem. Solids*, 11 (1959) 278.
7 J. H. PEARCE AND P. G. MARDON, *J. Sci. Instr.*, 36 (1959) 457.
8 G. K. WILLIAMSON, D. M. POOLE AND J. A. C. MARPLES, *J. Inst. Metals*, 85 (1957) 431.
9 A. S. COFFINBERRY AND M. B. WALDRON, *Progress in Nuclear Energy*, Vol. I, Series V, Pergamon Press, London, 1956, p. 403.
10 P. G. MARDON, Private communication to M. B. WALDRON reported in "The Chemistry & Metallurgy of Neptunium", *Proc. Intern. Conf. Peaceful Uses Atomic Energy, Geneva*, 28 (1958) 299.
11 F. W. SCHONFELD, *Phase Diagrams studied at Los Alamos*, Plutonium Session, 2nd World Metallurgical Congress, Chicago, 1957. To be published by Am. Soc. Metals.
12 P. G. MARDON, Private communication to M. B. WALDRON reported in *Phase Diagrams studied at Harwell*, Plutonium Session, 2nd World Metallurgical Congress, Chicago, 1957. To be published by Am. Soc. Metals.
12 F. A. ROUGH AND A. A. BAUER, *U.S. Report B.M.I.* 1300. Published by Battelle Memorial Institute, Columbus, Ohio, 1958.
14 A. A. BOCHVAR, S. T. KONOBEEVSKY, V. I. KUTAITSEV, I. S. MENSHIKOVA AND N. T. CHEBOTAREV, *Proc. Intern. Conf. Peaceful Uses Atomic Energy, Geneva*, 6 (1958) 184.
15 P. G. MARDON, *Unpublished work.*
16 R. G. COPE, *Private communication.*

DEFORMATION OF A DUPLEX TITANIUM ALLOY

J. SUITER

Commonwealth Scientific and Industrial Research Organization, Baillieu Laboratory, University of Melbourne (Australia)

(Received January 6th, 1960)

SUMMARY

The deformation of a titanium alloy containing 6% aluminium and 4% vanadium has been studied. It is shown that on the average the grains of the primary alpha phase were subjected to less deformation than the specimen. From these observations it is concluded that the phenomenon of "beta embrittlement" in heat-treated titanium alloys is not due to increased deformation of the beta phase as a result of the elimination of the relatively soft alpha grains.

Although titanium alloys are reasonably ductile after quenching from temperatures higher than the beta transus, the ductility of most alloys drops sharply following ageing treatments at lower temperatures. In many alloys this phenomenon of "beta embrittlement" starts to become evident after solution treatment at temperatures just below the beta transus when the amount of alpha phase present at the solution temperature (primary alpha phase) is less than some 10%[1].

In the present experiments the relation between the deformation of samples subjected to various heat treatments and the deformation of the primary alpha grains has been studied to provide further information on the problem of beta embrittlement.

EXPERIMENTAL PROCEDURES

The material used in the experiments was nominally titanium–6% aluminium–4% vanadium in the form of sheet about 0.07" thick. Samples were solution treated for $3\frac{1}{2}$ h at 870, 930 and 960°C to produce structures which contained 45, 25 and 2% respectively of primary alpha phase. After solution treatment the samples were water quenched and some were then aged for 16 h at 550°C.

Samples in both the as quenched and aged condition were deformed by cold rolling. Aged samples quenched from 960°C cracked badly after more than 7% reduction in thickness and only small pieces could be given further reductions. Specimens from the rolled strip were polished in a plane normal to the rolling plane and parallel to the rolling direction and etched in 20% NaOH + 15% H_2O_2.

By means of an ocular micrometer the ratio of length to thickness was measured for 128 grains of primary alpha phase in each specimen. Assuming no lateral spread in the rolled strip the mean strain in the primary alpha grains was calculated from the length-to-thickness ratio before and after rolling.

References p. 479

Due to the statistical nature of the experiment precise values of the strain in the primary alpha grains cannot be quoted. As an indication of the experimental errors the 90% confidence limits for the mean strains have been calculated by standard statistical procedure, *i.e.* there is a 90% probability that the true mean strain lies within the indicated ranges.

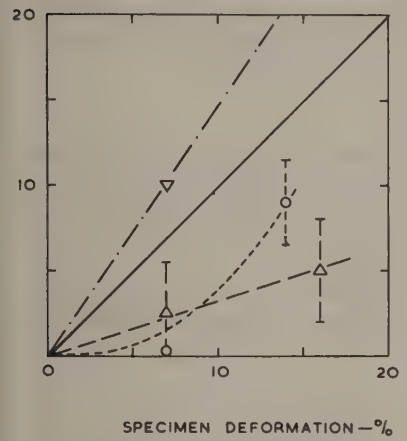

Fig. 1. Deformation of Ti–6%Al–4%V solution treated at 870°C, containing 45% primary alpha phase. —— Homogeneous solid. o– – – – –o alpha phase (w.q). Δ— —Δ alpha phase (age). ▽— · —▽ beta phase (age).

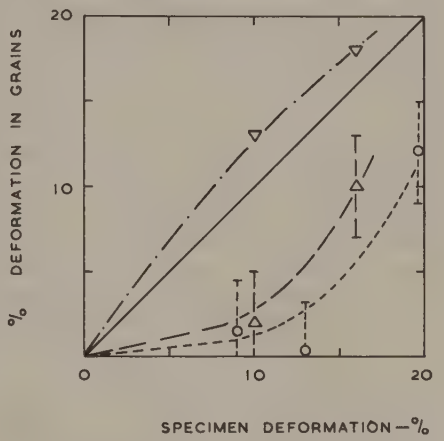

Fig. 2. Deformation of Ti–6%Al–4%V solution treated at 930°C, containing 25% primary alpha phase. —— Homogeneous solid. o– – – – –o alpha phase (w.q). Δ— —Δ alpha phase (age). ▽— · —▽ beta phase (age).

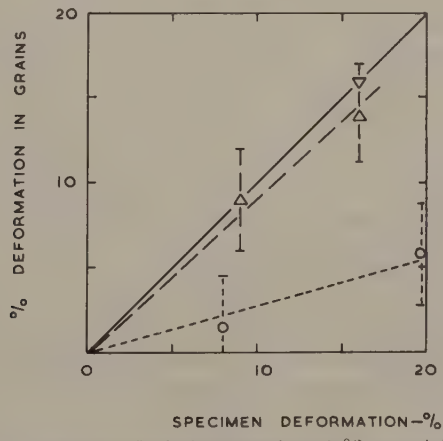

Fig. 3. Deformation of Ti–6%Al -4%V solution treated at 960°C, containing 2% primary alpha phase. —— Homogeneous solid. o– – – – –o alpha phase (w.q). Δ— —Δ alpha phase (age). ▽— · —▽ beta phase (age).

References p. 479

RESULTS

Figs. 1, 2 and 3 show the deformation of the primary alpha grains as a function of the specimen deformation after various heat treatments. In each case the deformation of the alpha grains is less than the overall deformation of the specimen. In the as quenched condition, as the amount of primary alpha phase decreases from 45% to 2% the deformation of the primary alpha grains decreases slightly. However in the aged condition the deformation of the primary alpha grains increases with decreasing amounts of primary alpha phase until it is almost identical with the specimen deformation when there is only 2% of primary alpha phase present.

DISCUSSION

In other duplex alloys it has been found[2,3] that when the minor phase was harder than the matrix the ratio of deformation of the minor phase to overall deformation decreased as the amount of the minor phase decreased. However, when the minor phase was softer than the matrix the deformations in the two phases were identical and independent of the amount of the minor phase.

Considering the alloys in the as quenched condition the primary alpha grains are harder than the beta grains (mixture of retained beta and martensitic alpha) and, as in the other work cited above, the deformation of the harder second phase decreases with decreasing amounts of the second phase.

However, in the aged condition the primary alpha phase is softer than the matrix and it might be expected that the alpha grains would be deformed to the same extent as the matrix. Although this occurs when there is only 2% of primary alpha phase the deformation of the primary alpha grains decreases with increasing amounts of primary alpha phase. If the hardness of aged beta phase decreases with decreasing solution temperature so that it approaches the hardness of the primary alpha phase then the present results can be explained. Such a change in hardness is not unexpected for the composition of the phases varies with the solution temperature. This effect will be more marked in the aged beta phase than in either the primary alpha or quenched beta phases since the ageing reactions are very sensitive to changes in composition of the beta phase whereas the properties of the primary alpha and the quenched beta phases change only slowly with composition.

For the aged alloys the deformation of the beta grains has been calculated from the deformation of the primary alpha grains and the amount of primary alpha phase. The deformation of the aged beta phase is shown in Figs. 1, 2 and 3. For a given specimen deformation this shows that the deformation of the aged beta grains decreases with increasing solution temperature. From this it appears that beta embrittlement is not due to increased deformation of the beta phase as a result of the elimination of the relatively soft alpha grains.

However, in the present experiments only the average deformation of the primary alpha grains has been measured. No estimate can be made of any inhomogeneous deformation within these grains that may assist in transmitting the strain from one beta grain to the next and so prevent the formation of grain boundary cracks.

ACKNOWLEDGEMENTS

The investigation formed part of the programme of research of the Physical Metal-

References p. 479

lurgy Section of the Commonwealth Scientific and Industrial Research Organization, Australia. The work was carried out at the Baillieu Laboratory, University of Melbourne, under the general direction of Professor H. W. WORNER, to whom the author expresses his thanks.

REFERENCES

[1] A. J. WILLIAMS, *Can. Dept. Mines and Tech. Surveys Research Rept.* R11, 1958.
[2] L. M. CLAREBOROUGH, *Australian J. Sci. Research Ser. A*, 3 (1950) 72.
[3] L. M. CLAREBOROUGH AND G. E. PERGER, *Australian J. Sci. Research Ser. A*, 5 (1952) 114.

THE NIOBIUM–RHENIUM SYSTEM

A. G. KNAPTON

Associated Electrical Industries, Aldermaston, Berks. (Great Britain)

(Received January 13th, 1960)

SUMMARY

The constitutional diagram of the niobium–rhenium system has been determined over the whole range of compositions. Two intermediate phases occur in the system, one with the sigma structure (σ) and the other an α-manganese type (χ). The sigma phase is formed peritectically at 57 at-% rhenium and exists over only a small range of compositions and temperatures. The chi (χ)-phase melts congruently at 2800°C and has a homogeneity range of 62–87% rhenium, which falls little with decreasing temperature. Niobium dissolves up to 46 at-% rhenium at the eutectic temperature, falling to 43% at 1000°C. The solubility of niobium in solid rhenium is low.

INTRODUCTION

In spite of the considerable technological interest in the refractory transition metals, many of their alloys remain unexplored. As part of our general study of alloy behaviour, an investigation has been made of the niobium–rhenium system. This system was selected to yield further information on the alloying of rhenium metal, and to form a useful comparison with the molybdenum–rhenium system described earlier[1,2]. Both molybdenum and niobium are elements of the Second Long Period of the Periodic System, and the intermediate phases present in the two systems are the same. Consequently, it was anticipated that information on relative terminal solubilities and stabilities of the intermediate phases would be of value in further understanding the alloying behaviour of these metals, and would allow further generalisations to be made concerning transition metal alloys.

TABLE I

PUBLISHED LATTICE SPACINGS OF NIOBIUM–RHENIUM PHASES

Sigma phase		*α-Manganese (χ) phase*		*Reference*
Alloy composition	*Lattice spacing (Å)*	*Alloy composition*	*Lattice spacing (Å)*	
50 at-% Re	$a = 9.78$ (3) $c = 5.11$ (5)	75 at-% Re	$a = 9.683$	(3)
59 at-% Re	$a = 9.72$ $c = 5.07$	—	$a = 9.670$	(4)
—	—	$Re_{22}Nb_7$ = 76 at-% Re	$a = 9.676$	(5)

References p. 486

Previous work on niobium–rhenium alloys by the present author[3] and by GREENFIELD AND BECK[4] showed the presence of two intermediate phases in the system, one with the sigma structure (σ), the other with the α-manganese (χ) structure. The sigma phase was shown to exist at elevated temperatures only[3]. NIEMIEC AND TRZEBIATOWSKI[5] reported lattice spacing measurements for the χ phase, which was designated $Re_{22}Nb_7$ by these authors on the basis of 58 atoms per unit cell for the α-manganese structure. These and other lattice spacing measurements made previously are collected in Table I.

No phase diagram of the niobium–rhenium system has appeared in the literature.

EXPERIMENTAL PROCEDURE

All alloys were prepared by arc melting in an atmosphere of gettered argon. Beads of 2–4 g in weight were melted, turned over and remelted several times to ensure homogeneity. Weight losses on alloying were small ($< 0.5\%$), and synthesised compositions have been used in the bulk of this work. The results of chemical analyses on selected alloys (Table II) justify this.

TABLE II

CHEMICAL ANALYSIS OF CERTAIN ALLOYS

Composition (wt-% Re)		*Composition (wt-% Nb)*	
Synthesised	*Analysed*	*Synthesised*	*Analysed*
96.9	97.0	3.1	—
69.5	70.1	30.5	30.1
66.5	66.4	33.5	33.6
78.4	78.2	21.6	21.3
61.7	61.4	38.3	38.9

Both niobium and rhenium were supplied by Johnson Matthey and Co., Ltd. The niobium was in the form of spectrographically standardised "H.S." rods containing traces of zirconium, tantalum, silicon and iron as the principal impurities. The rhenium was in powder form with a purity $> 99.5\%$ rhenium. The metals were arc melted prior to being used for alloying.

Liquidus determinations were made by the technique previously described[6]. The values obtained cannot be claimed to represent accurate liquidus measurements, but are considered as a good approximation.

Annealing of small sections of alloy beads was performed in a niobium block in the argon arc furnace. The method was suitable for anneals in the 1800–2400°C range, and has been described in an earlier paper[6]. When necessary the annealing block was quenched by flooding the arc furnace chamber with water at the end of the annealing operation.

Annealing at lower temperatures was carried out *in vacuo* in high frequency or platinum resistance furnaces.

Conventional metallographic methods involving final polishing with diamond dust on Selvyt cloth were employed for the niobium–rhenium alloys. Structures of duplex and intermediate compound alloys were revealed by etching in a 1 : 1 : 1 mixture

References p. 486

of hydrofluoric acid, nitric acid and water. For niobium-rich alloys, this etchant was slow and the water content was reduced for etching.

Powder photographs were taken in a 9 cm Unicam X-ray camera using copper or chromium Kα radiation. Alloys in the range 15–90 at-% rhenium were sufficiently brittle to be readily powdered in a mortar and pestle.

RESULTS

The niobium–rhenium diagram proposed from the results of this investigation is given in Fig. 1, together with the experimental observations on which the diagram is based. The liquidus values show a flat minimum near 50 at-% rhenium (Table III), corresponding to the eutectic between the niobium-base solid solution and sigma (σ).

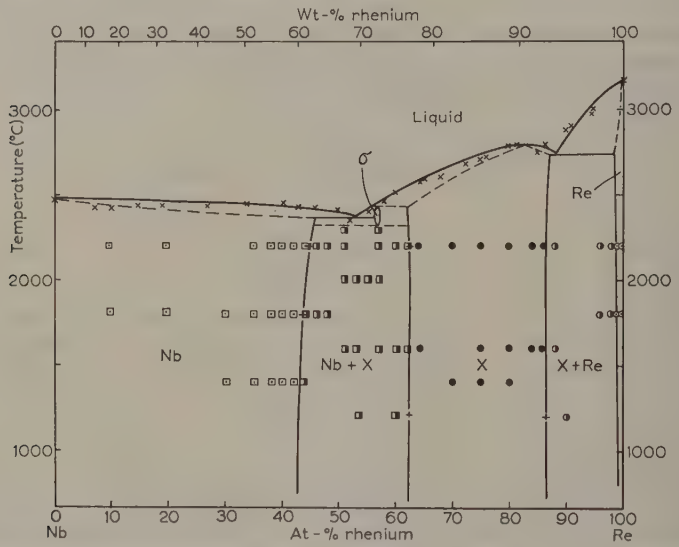

Fig. 1. The Nb–Re system: ⊡, Nb; ◨, Nb + χ; ●, χ; ◑, χ + Re; ◎, Re; ×, Melting points; +, X-ray solubilities.

The depression of the niobium freezing point on alloying is small, the eutectic being estimated at 2400°C compared with the niobium melting point 2468°C[7]. A further small minimum occurs near 88 at-% rhenium, the eutectic composition between rhenium and the χ phase. The χ phase melts congruently at 2800°C, and the χ/rhenium eutectic temperature has been placed at 2730°C.

Metallographic studies of arc-cast alloys confirm the mode of formation of the intermediate phases shown in Fig. 1. The sigma phase forms peritectically at 2450°C and 57 at-% rhenium and exists over a narrow composition range only. As melted alloys containing 55–60 at-% rhenium consisted of three phases. The microstructure of a 60 at-% rhenium alloy is given in Fig. 2, showing primary dendrites of the χ phase surrounded by a peritectic case of sigma with a small quantity of sigma–niobium solid solution eutectic.

References p. 486

TABLE III

MELTING POINTS OF NIOBIUM–RHENIUM ALLOYS

Composition (at-% Re)	*Melting point (°C)*	*Composition (at-% Re)*	*Melting point (°C)*
0	2468[7]	60	2510
7	2420	64.2	2580
10	2420	65	2590
14.5	2430	68	2600
19	2430	72.3	2680
27	2430	75	2700
34	2450	76	2720
38	2450	80	2790
40.3	2450	81.2	2790
43	2420	85	2750
46	2420	86.3	2790
50	2410	90	2870
52	2350	90.8	2900
55.1	2400	94.7	2980
57.9	2460	95	3000
		100	3180

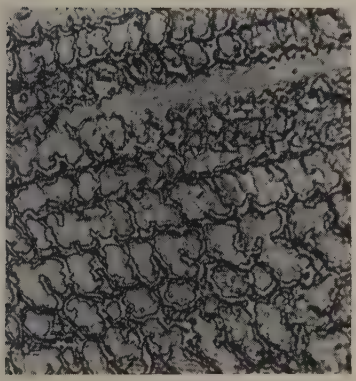

Fig. 2. 60 at-% rhenium, as cast (× 500).

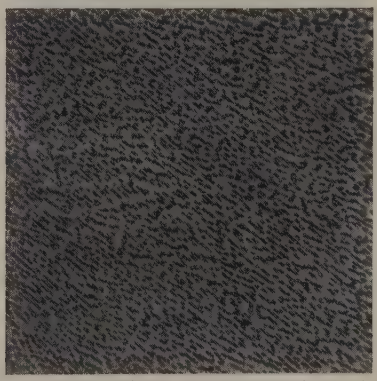

Fig. 3. 88 at-% rhenium, as cast (× 500).

The eutectic between rhenium and the χ phase occurs very close to the rhenium rich boundary of the χ phase. An arc melted alloy of 88 at-% rhenium showed a typical eutectic structure (Fig. 3) consisting of short lamellae of rhenium in a matrix of χ.

The solid solubility limits of the single phase regions were determined metallographically on annealed alloys and confirmed by lattice spacing measurements.

Rhenium dissolves extensively in niobium, as may be expected from the relative atomic diameters of the elements (Nb = 2.95 Å, Re = 2.76 Å). After annealing at 2200°C, an alloy containing 44 at-% rhenium was single phase niobium solid solution, whereas a 46 at-% alloy was duplex (Fig. 4). The maximum solubility of rhenium in niobium has consequently been placed at 46 at-% rhenium, which is in good agreement with the value obtained by X-ray methods (Table IV, Fig. 5). The solubility of rhenium in niobium in the solid state is little affected by temperature, falling to *ca.* 43 at-% rhenium at 1000°C.

References p. 486

TABLE IV

LATTICE SPACINGS OF NIOBIUM-BASE SOLID SOLUTIONS

Composition (at-% Re)	*Heat treatment (Annealing)*	*Lattice spacing (Å)*
9.8	1800°C, 5 h	3.274
19.5	1800°C, 5 h	3.248
19.5	1900°C, 5 h	3.247
30	2200°C, 2 h	3.224
35	2200°C, 2 h	3.212
38	2200°C, 2 h	3.207
44.5	2200°C, 2 h	3.196
44.5	1200°C, 3 days	3.195
50	2200°C, 2 h	3.194
51	2200°C, 2 h	3.194
51	1800°C, 5 h	3.195
57	2200°C, 2 h	3.194
57	1800°C, 5 h	3.198

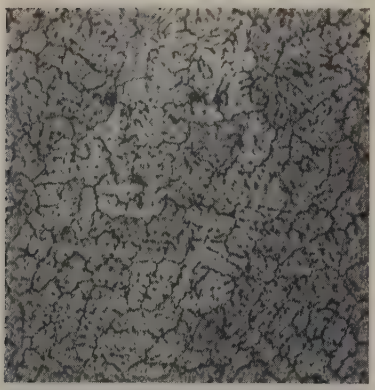

Fig. 4. 46 at-% rhenium, annealed 2200°C (× 100).

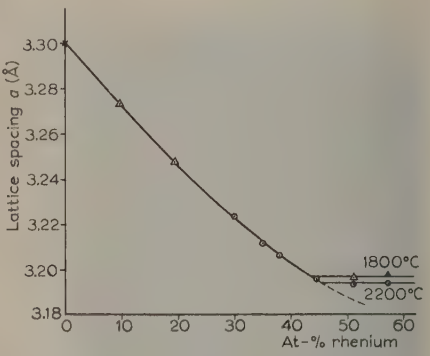

Fig. 5. Lattice spacings of Nb-base solid solutions: o, 2200°C; △, 1800°C.

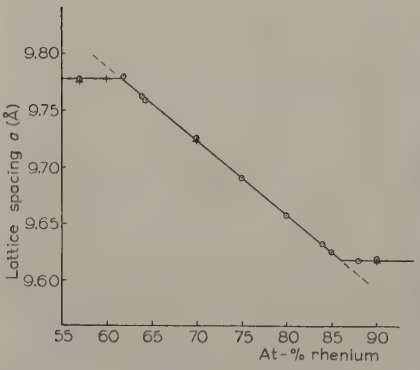

Fig. 6. Lattice spacings of the Nb–Re χ phase: o, 2200°C; +, 1200°C.

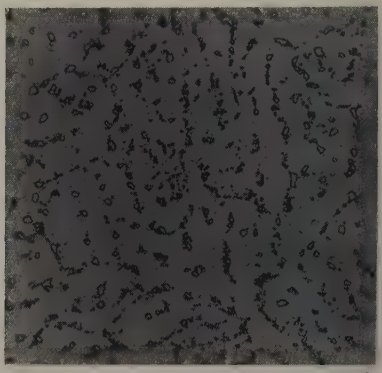

Fig. 7. 98 at-% rhenium, annealed 1800°C (× 300).

TABLE V

LATTICE SPACINGS OF CUBIC χ PHASE

Composition (at-% Re)	*Heat treatment*	*Lattice spacing (Å)*
57	Annealed 2200°C, 5 h	9.779
62		9.780
64		9.762
64.2		9.760
70		9.726
75		9.690
80		9.659
84		9.632
85		9.626
88		9.617
90		9.619
57	Annealed 1200°C, 28 days	9.778
60		9.778
70		9.725
90		9.617

The sigma phase in this system has been detected by X-ray and metallographic methods in as melted alloys only, and is considered to exist over a very narrow range of compositions and temperatures. Specimens containing 51 and 57 at-% rhenium were water quenched from successively higher temperatures in the range 2000–2300°C. In all of these specimens, the phases detected by X-ray powder photography were χ and the niobium-base solid solution.

Samples containing a high proportion of the χ phase were sufficiently brittle to give well-resolved powder photographs without stress relieving anneals of the powder. Lattice spacing measurements from heat treated lump specimens are given in Table V, and plotted in Fig. 6. In the single phase region, the lattice spacings vary almost linearly with composition. The X-ray solubilities give a homogeneity range for the compound of 62–86 at-% rhenium. Little change of lattice spacing of the two-phase alloys (χ + Re, or χ + Nb) could be detected on annealing at lower temperatures. Metallographic examination confirmed the X-ray results, and has bracketted the boundaries between 62 and 64 at-% rhenium on the niobium side at 2200°C, and between 86 and 88 at-% rhenium in rhenium-rich alloys.

The solubility of niobium in rhenium in the solid state is low. Arc melted alloys of 2 at-% niobium contained appreciable quantities of second phase. After annealing in a niobium block at 2200°C for 5 h, an alloy containing 1 at-% niobium was single phase and a 2 at-% alloy duplex. The maximum solid solubility has been placed at 1.5 at-% niobium, and does not fall below 1 at-% at 1800°C. Fig. 7 shows a 98 at-% rhenium alloy annealed at 1800°C.

CONCLUSIONS

(1) The maximum solid solubility of rhenium in niobium is 46 at-% at the eutectic temperature falling to 43 at-% at 1000°C.

(2) The sigma phase (σ) exists over a small range of compositions and temperatures.

(3) The chi phase (χ) has a wide homogeneity range, 62–87 at-% rhenium, and melts congruently at 2800°C.

References p. 486

(4) The maximum solid solubility of niobium in rhenium is low, *ca.* 1.5 at-%.

(5) Two eutectics occur in the system, one at 2400°C, 53 at-% rhenium between sigma and the niobium solid solution, the other at 2730°C, 88 at-% rhenium, between chi (χ) and rhenium.

ACKNOWLEDGEMENTS

The author wishes to thank Dr. G. A. GEACH for his encouragement and interest in the work, and Dr. T. E. ALLIBONE, F.R.S., Director of the Laboratory, for permission to publish this paper.

REFERENCES

1 A. G. KNAPTON, *Associated Electrical Industries Research Rept.* No. A. 736, 1957.
2 A. G. KNAPTON, *J. Inst. Metals*, 87 (1958–59) 62.
3 A. G. KNAPTON, *J. Inst. Metals*, 87 (1958–59) 28.
4 P. GREENFIELD AND P. A. BECK, *Trans. AIME*, 206 (1956) 265.
5 J. NIEMIEC AND W. TRZEBIATOWSKI, *Bull. acad. polon. sci.*, Classe III, 4 (1956) 601.
6 F. O. JONES, A. G. KNAPTON AND J. SAVILL, *J. Less-Common Metals*, 1 (1959) 80.
7 J. H. SCHOFIELD, *J. Inst. Metals*, 85 (1956–57) 372.

Book Reviews

Internal stresses and fatigue in metals, edited by G. M. Rassweiler and W. L. Grube, Elsevier Publishing Co., Amsterdam, 1959, 451 pages, £3 12s.

This book is a compilation of a series of twenty-four papers presented as a Symposium on Internal Stresses and Fatigue, organized by the General Motor Research Laboratories in Detroit in 1958. The purpose of the Symposium was to consider and interrelate the phenomena of internal stresses and fatigue in metals from the point of view of the atomic and the solid-state physicist, and to attempt to answer such questions as, what causes and influences internal stress and fatigue in metals, and where do the lines of approach to these problems followed by the engineer and the metal physicist come together. The field is covered under the headings of concepts and significance of internal stresses; crystal lattices, imperfections, and stresses; dislocations, internal stresses and fatigue; and fatigue and related phenomena.

Much has been written on these subjects and there are still some aspects of them which are not fully understood. This new book reviews in detail the relevant information now available, and the practical significance of internal stress and fatigue. Both have many facets, and one of the attractions of this book is its breadth of treatment. Appreciation of the causes and effects of internal stress is necessary for a proper understanding of its significance in engineering applications, and similarly increase in fatigue life can only be achieved if the causes of fatigue failure in practice can be defined. These are merely examples of the type of information provided, but the book goes much further; and in addition to discussion of fundamentals consideration is, for instance, given to the techniques available for the study of the phenomena involved, and to ancillary matters such as the time-dependent embrittling effect of hydrogen on steel and its influence in static fatigue, and the effects of internal and applied stress on the chemical properties, and hence on the mode of corrosion, of ferrous metals and stainless steels.

The book is considerably more comprehensive than its title might appear to indicate. However, all the information it contains is directly or indirectly relevant, and the inclusion of so much data in a single volume is to be commended.

Clarity of exposition is evident throughout, and it is obvious that much careful thought has been given to the choice of the topics presented. The book includes a useful summary of the Symposium papers.

J. W. C.

Friction and wear, edited by R. Davies, Elsevier Publishing Co., Amsterdam, 1959, 191 pages, £1 16s 6d.

This book, which covers the Proceedings of the Symposium on Friction and Wear, organized by the General Motors Research Laboratories in Detroit in 1957, should readily appeal to all those interested in the fundamental and practical implications of these very important subjects.

The demand for longer life and greater reliability from internal combustion engines and other engineering components is enforcing closer control over the wear and friction of moving parts, and such control can properly be exercised only when the basic mechanisms of these processes are understood. Recent advances in solid state and surface state physics have shed more light on the nature of friction and wear, and phenomena such as stick-slip, seizure under boundary lubrication, wettability, and the adsorption of monomolecular films, which are amongst those topics considered in this book, can now be more rationally explained. Likewise the metallurgical aspects of friction and wear have now become clarified and under this heading useful information is provided on the sliding characteristics for various metallic couples, including some metals that come particularly within the terms of reference of this Journal. It is not however necessary to offer this as an excuse for publishing this review, as although friction and wear may not interest all our readers they are undoubtedly the serious concern of others, for instance, those interested in the engineering uses of titanium.

The book contains a considerable amount of fundamental information, and the inclusion of the discussions, although presumably abridged, following the presentation of the various papers that form its individual sections, adds considerably to their value. Each section in consequence is a remarkably good summary of the latest information on its particular aspect of these two important subjects, and the book as a whole covers them in a masterly fashion. The result is a compilation that should be of considerable value to the engineer and others who may be concerned with the problems of combating friction and reducing wear.

J. W. C.

AUTHOR INDEX

ANTILL, J. E. AND K. A. PEAKALL 227
ARMSTRONG, D. J., D. MURRAY AND L. M. T. HOPKIN 125
BATES, B., see WOOLLEY, J. C.
BELK, J. A. 50
BICKERDIKE, R. L. AND G. HUGHES . . . 42
BRADSHAW, F. J. AND C. WHEELER. . . . 101
BRASIER, J. AND W. HUME-ROTHERY. . . 157
BRAUN, H., K. SEDLATSCHEK, AND R. KIEFFER. 413
——, see KIEFFER, R.
BROWN, A. R. G., D. CLARK AND J. EASTABROOK. 94
BROWN, S. A. AND J. E. LAND 237
CAMPBELL, I. E., D. M. ROSENBAUM AND B. W. GONSER 185
CLARK, D., see BROWN, A. R. G.
COWLEY, A. H., see FAIRBROTHER, F.
EASTABROOK, J., see BROWN, A. R. G.
FAIRBROTHER, F., A. H. COWLEY AND N. SCOTT 206
FERRO, R. 424
FITZGERALD, L. M., see MORDIKE, B. L.
GEACH, G. A. AND F. O. JONES. 56
GILBEY, D.M. 139
GONSER, B. W. see CAMPBELL, I. E.
GROSS, P., D. L. LEVI AND G. L. WILSON . 113
HALL, R. O. A., see LEE, J. A.
HAWORTH, C. W. 106
HELLAWELL, A. 110, 343
HILL, D. L., see MENZIES, I. A.
HOLMES, P. J., see WOOLLEY, J. C.
HOPKIN, L. M. T., see ARMSTRONG, D. J.
HUGHES, G., see BICKERDIKE, R. L.
HUGHES, J. E. 377
HUME-ROTHERY, W., see BRASIER, J.
——, see ROSS, R. G.
JACQUET, P.-A. 439
JOHANSEN, H. A. AND R. C. MILLER . . . 331
JONES, F. O., A. G. KNAPTON AND J. SAVILL. 80
— —, see GEACH, G. A.
JUNG-KÖNIG, W., see SCHLEICHER, H. W.
KIEFFER, R., K. SEDLATSCHEK AND H. BRAUN. 19
——, see BRAUN, H.
KNAPTON, A. G. 480
——, see JONES, F.O.
KNIGHT, J. R. AND D. W. RHYS 292
KRISTJANSON, A. M. AND M. LEDERER . . 245
LAND, J. E., see BROWN, S. A.
LEDERER, M., see KRISTJANSON, A. M.
——, see SHUKLA, S. K.
LEE, J. A. AND R. O. A. HALL 356
LEES, D. G., see WOOLLEY, J. C.
LEVI, D. L., see GROSS, P.
LIVEY, D. T. 145
MACKOWIAK, J. AND L. L. SHREIR 456
MARDON, P. G. AND J. H. PEARCE 467
MARTIN, A. J. AND A. MOORE 85
MEHROTRA, R. C., see VERMA, I.D.
MENZIES, I. A., D. L. HILL AND L. W. OWEN 321
MERKEL, H. 390
MILLER, R. C., see JOHANSEN, H. A.
MOORE, A., see MARTIN, A. J.
MORDIKE, B. L. AND L. M. FITZGERALD . . 132
MOSS, A. R. 34, 60
MURRAY, D., see ARMSTRONG, D. J.
MURRAY, J. R. 314
—— AND G. K. WILLIAMSON 73
OLDFIELD, W. 77
OWEN, L. W., see MENZIES, I. A.
PAMPLIN, B. R., see WOOLLEY, J. C.
PEAKALL, K. A., see ANTILL, J. E.
PEARCE, J. H., see MARDON, P. G.
PICKMAN, D. O. AND E. W. WARD 116
RAUB, E. 3
RAYNOR, G. V., see WEINER, R. T.
REA, T. W., see WILMS, G. R.
RHYS, D. W. 269
——, see KNIGHT, J. R.
ROBINS, D. A. 396
ROSENBAUM, D. M., see CAMPBELL, I. E.
ROSS, R. G. AND W. HUME-ROTHERY. . . 304
SAMBELL, R. A. J., see WILLIAMS, J.
SAVILL, J., see JONES, F. O.
SCHLEICHER, H. W. AND W. JUNG-KÖNIG . 348
SCHREIR, L. L., see MACKOWIAK, J.
SCOTT, N., see FAIRBROTHER, F.
SEDLATSCHEK, K., see BRAUN, H.
——, see KIEFFER, R.
SHUKLA, S. K. 333
—— AND M. LEDERER 202, 255
SMITH, B. A., see WOOLLEY, J. C.
SUITER, J. 232, 476
VERMA, I. D. AND R. C. MEHROTRA. . . . 263
WARD, E. W., see PICKMAN, D. O.
WEINER, R. T. AND G. V. RAYNOR 309
WHEELER, C., see BRADSHAW, F. J.
WILLIAMS, J. AND R. A. J. SAMBELL . . . 217
WILLIAMSON, G. K., see MURRAY, J. R.
WILMS, G. R. AND T. W. REA 152, 411
WILSON, G. L., see GROSS, P.
WOOLF, A. A. 420
WOOLLEY, J. C. AND B. BATES. 382
—— AND D. G. LEES 192
——, D. G. LEES AND B. A. SMITH 199
——, B. R. PAMPLIN AND P. J. HOLMES . . 362
ZWICKER, U. 165

SUBJECT INDEX

Aluminium, liquid, interaction layers with solid Ti 456
—, properties of alloys with Ti–Nb . . . 232
Antimony, equilibrium diagrams with InSb as one component 192
Arc-furnaces, techniques for study of refractory metals 80
Arc-melting, processes for refractory metals 60
Beryllium, electrodeposition from non-aqueous solutions 321
——, structure of, especially at high temperatures 85
Bismuth, equilibrium diagram of Bi–Pd system. 157
—, study of compound Bi_4Rh 304
Cerium, metallic, transformations in . . . 309
Chromium, atmospheric contamination of 152
——, loss of metal at elevated temperatures in air 411
——, mechanical properties. 152
Cobalt, ordering in CoPt–FePt alloys . . . 382
Cooling curves, molybdenum resistance furnace for 77
Creep testing, techniques at high temperatures 125
Electron bombardment, techniques for study of refractory metals. 80
Ellopol technique 439
Furnace(s), for study of high temperature equilibria. 106
——, molybdenum resistance, for cooling curves 77
Gadolinium, equilibrium diagram of Gd_2Te_3–In_2Te_3 system 199
Gallium, purification with ammonia . . . 390
High temperature(s), furnaces for study of —— —— equilibria 106
—— ——, mechanical working of arc-cast molybdenum at 116
—— ——, stability of oxides and sulphides at. 145
—— ——, techniques, in alloy investigations 73
Indium, equilibrium diagram of Ga_2Te_3–In_2Te_3 system. 199
——, equilibrium diagrams with InSb as one component 192
——, ordered crystal structure of In_2Te_3 . 362
——, system with Pd. 292
Iron, ordering in CoPt–FePt alloys . . . 382
——, solid state transitions in solid solutions. 110
Magnesium, micrographic examination of alloys with Pd. 424
——, X-ray examination of alloys with Pd. 424
Manganese, alloys with second transition series metals 343
——, solid state transitions in solid solutions. 110
Mechanical properties, effect of atmospheric contamination on —— —— of Cr. 152
—— ——, methods of measuring —— —— of solids at high temperatures 132
Molybdenum, grain structure of as-cast ingots 34
—— high temperature mechanical working of arc-cast —— 116
——, zone refining of. 50
Neptunium, equilibrium diagram of Np–U system. 467
Niobium, alloys with Ta 413
—— (V), oxytrichlorides and oxytribromides of 206
——, properties of Ti–Al–Nb alloys. . . . 232
——, spectrophotometric investigation of complex with protocatechuic acid . 237
Oxides, high temperature stability of . . . 145
Palladium, equilibrium diagram of Pd–Bi system. 157
——, micrographic examination of Mg–Pd alloys 424
—, system with In 292
——, system with Sn. 292
——, X-ray examination of Mg–Pd alloys . 424
Platinum, metals and alloys of —— group . 3
——, ordering in CoPt–FePt alloys. . . . 382
Plutonium metal, thermoelectric power of. 356
Polishing, local electrolytic, for Be, Zr, Mo. 439
Pyrolytic carbon, deformation of deposited ——— ——— 101
—— ——, structure and density of . . . 94
Refractory metals, arc furnace and electron bombardment techniques for study of 80
—— ——, arc-melting processes for . . . 60
—— ——, zone melting of 56
Rhenium, analysis of its alloys 420
——, availability of 185
——, recovery of 185, 420
——, properties of. 185
——, system with carbon 377
——, zone melting of. 56
Rhodium, the compound Bi_4Rh 304
Rhodium(III), solution chemistry of sulphates 255
—— —, solution chemistry in 6 *N* HCl . . 245
—— —, study of oxalates by paper electrophoresis, paper chromatography, ion-exchange chromatography and spectrophotometry 333
——— —, study of perchlorate by paper electrophoresis and spectrophotometry 202
Ruthenium, fabrication of 269

——, properties of 269
Sulphides, high temperature stability of. . 145
Tantalum, alloys with Nb. 413
—— (V), oxytrichlorides and oxytribromides of 206
Thermal stresses, theory of 139
Thermodynamic activities, methods for determining —— —— of alloy constituents at high temperatures. . . 113
Thorium, Th-rich Th–In alloys 314
Tin, system with Pd 292
Titanium, deformation of Duplex alloy . . 476
——, development of heat-resistant alloys. 165
——, effect of H on hot-workability of alloys with Al. 348
Titanium, examination of part of Ti–C system. 42
——, properties of Ti–Al–Mo alloys. . . . 232
——, reactions between isopropyl titanate and acetyl bromide 263
——, solid, interaction layers with liquid Al. 456
Transition metals, properties of 396
Tungsten, high melting point alloys . . . 19
——, zone melting of. 56
Uranium, equilibrium diagram Np–U system 467
——, kinetics of oxidation by carbon dioxide. 227
——, monocarbide–mononitride system . 217
Yttrium, Seebeck coefficient from 0–1000°C. 331
Zone melting of refractory metals 56
Zone refining of Mo 50

CONTENTS

Untersuchungen an Niob–Tantal-Legierungen
von H. Braun, K. Sedlatschek und R. Kieffer (Reutte/Tirol) 413

The recovery of rhenium and the analysis of its alloys
by A. A. Woolf (Aldermaston) 420

Research on the alloys of noble metals with the more electropositive elements. II. Micrographic and roentgenographic examination of the magnesium–palladium alloys
by R. Ferro (Genoa). 424

Polissage électrolytique local (technique „Ellopol") pour la métallographie du béryllium, du zirconium et du molybdène
par P.-A. Jacquet (Paris). 439

The nature and growth of interaction layers formed during the reaction between solid titanium and liquid aluminium
by J. Mackowiak and L. L. Shreir (London). 456

An investigation of the neptunium–uranium equilibrium diagram
by P. G. Mardon and J. H. Pearce (Harwell) 467

Deformation of a duplex titanium alloy
by J. Suiter (Melbourne). 476

The niobium–rhenium system
by A. G. Knapton (Aldermaston) 480

Book Reviews. 487

Author Index 488

Subject Index 490

All rights reserved

ELSEVIER PUBLISHING COMPANY, AMSTERDAM

Printed in The Netherlands by

NEDERLANDSE BOEKDRUK INRICHTING N.V., 'S-HERTOGENBOSCH

FILED IN STACKS

ELSEVIER'S

SCIENTIFIC JOURNALS

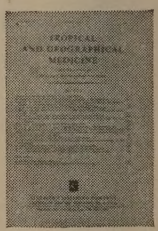

ANALYTICA CHIMICA ACTA

BIOCHIMICA ET BIOPHYSICA ACTA

JOURNAL OF CHROMATOGRAPHY

CLINICA CHIMICA ACTA

ICSU REVIEW

TROPICAL AND GEOGRAPHICAL MEDICINE

EPILEPSIA

JOURNAL OF ELECTROANALYTICAL CHEMISTRY

WEAR - USURE - VERSCHLEISS

Specimen copies are available

ELSEVIER PUBLISHING COMPANY
110-112 SPUISTRAAT — AMSTERDAM — THE NETHERLANDS